Check for updates

The Meteoritical Society

Meteoritics & Planetary Science 59, Nr 4, 719–753 (2024)
doi: 10.1111/maps.14066

Enstatite meteorite clasts in Almahata Sitta and other polymict ureilites: Implications for the formation of asteroid 2008 TC_3 and the history of enstatite meteorite parent asteroids

Cyrena Anne GOODRICH[1]*, Hilary DOWNES[2,3,4], Richard GREENWOOD[5], Aidan J. ROSS[3,4,6], Anna Maria FIORETTI[7], Louise ALEXANDER[2], Noriko T. KITA[8], Jon BUTLER[2], Michael J. JERCINOVIC[9], Peter JENNISKENS[10], and Muawia H. SHADDAD[11]

[1]Lunar and Planetary Institute, USRA, Houston, Texas, USA
[2]Department of Earth and Planetary Science, Birkbeck University of London, London, UK
[3]Department of Earth Sciences, Natural History Museum, London, UK
[4]UCL/Birkbeck Centre for Planetary Sciences, University College London, London, UK
[5]School of Physical Sciences, Open University, Milton Keynes, UK
[6]Department of Earth Sciences, University College London, London, UK
[7]CNR—Istituto Scienze Polari, Padua, Italy
[8]WiscSIMS Laboratory, Department of Geosciences, University of Wisconsin-Madison, Madison, Wisconsin, USA
[9]Department of Geosciences, University of Massachusetts Amherst, Amherst, Massachusetts, USA
[10]SETI Institute, Mountain View, California, USA
[11]Department of Physics and Astronomy, University of Khartoum, Khartoum, Sudan
***Correspondence**
Cyrena Anne Goodrich, Lunar and Planetary Institute, USRA, 3600 Bay Area Boulevard, Houston, TX 77058, USA.
Email: goodrich@lpi.usra.edu

(Received 28 March 2023; revision accepted 02 August 2023)

Abstract–The anomalous polymict ureilite Almahata Sitta (AhS) fell in 2008 when asteroid 2008 TC_3 disintegrated over Sudan and formed a strewn field of disaggregated clasts of various ureilitic and chondritic types. We studied the petrology and oxygen isotope compositions of enstatite meteorite samples from the University of Khartoum (UoK) collection of AhS. In addition, we describe the first bona fide (3.5 mm-sized) clast of an enstatite chondrite (EC) in a typical polymict ureilite, Northwest Africa (NWA) 10657. We evaluate whether 2008 TC_3 and typical polymict ureilites have a common origin, and examine implications for the history of enstatite meteorite asteroids in the solar system. Based on mineralogy, mineral compositions, and textures, the seven AhS EC clasts studied comprise one EH_a3 (S151), one EL_b3 (AhS 1002), two EH_b4-5 (AhS 2012, AhS 26), two EH_b5-6 or possibly impact melt rocks (AhS 609, AhS 41), and one EL_b6-7 (AhS 17), while the EC clast in NWA 10657 is EH_a3. Oxygen isotope compositions analyzed for five of these are similar to those of EC from non-UoK collections of AhS, and within the range of individual EC meteorites. There are no correlations of oxygen isotope composition with chemical group or subgroup. The EC clasts from the UoK collection show the same large range of types as those from non-UoK collections of AhS. The enstatite achondrite, AhS 60, is a unique type (not known as an individual meteorite) that has also been found among non-UoK AhS samples. EC are the most abundant non-ureilitic clasts in AhS but previously were thought to be absent in typical polymict ureilites, necessitating a distinct origin for AhS. The discovery of an EC in NWA 10657 changes this. We argue that the types of materials in AhS and typical polymict ureilites are essentially similar, indicating a common origin. We elaborate on a model in which AhS and typical polymict ureilites formed in the same regolith on a ureilitic daughter body. Most non-ureilitic clasts are

© 2023 The Meteoritical Society.

remnants of impactors implanted at ~50–60 Myr after CAI. Differences in abundances can be explained by the stochastic nature of impactor addition. There is no significant difference between the chemical/petrologic types of EC in polymict ureilites and individual EC meteorites. This implies that fragments of the same populations of EC parent bodies were available as impactors at ~50–60 Myr after CAI and recently. This can be explained if materials excavated from various depths on EC bodies at ~50–60 Myr after CAI were reassembled into mixed layers, leaving relatively large bodies intact to survive 4 billion years. Polymict ureilites record a critical timestep in the collisional and dynamical evolution of the solar system, showing that asteroids that may have accreted at distant locations had migrated to within proximity of one another by 50–60 Myr after CAI, and providing constraints on the dynamical processes that could have caused such migrations.

INTRODUCTION

Polymict Ureilites and Almahata Sitta

Polymict ureilites are fragmental and regolith breccias that are interpreted to represent regolith developed on ureilitic asteroids, either the original ureilite parent body (UPB) or, more likely, rubble pile daughter bodies that were assembled in the aftermath of catastrophic disruption of the UPB (Downes et al., 2008; Goodrich et al., 2004; Goodrich, Hartmann, et al., 2015; Goodrich, Kring, et al., 2021; Goodrich, Sanborn, et al., 2021; Herrin et al., 2010). They consist dominantly of lithic and mineral clasts of various types of ureilites, but also contain up to ~10 vol% xenoliths—that is, clasts of non-ureilitic lithologies that are interpreted to be remnants of impactors. These xenoliths comprise a large range of meteorite types, including every major class of chondrite (OC, EC, RC, CC) with multiple subgroups and types of each, as well as several types of non-ureilitic achondrites (Bischoff et al., 2006; Boleaga & Goodrich, 2019; Downes et al., 2008; Goodrich et al., 2004, 2016; Goodrich, Fioretti, et al., 2015; Goodrich & Gross, 2015; Goodrich, Kita, et al., 2017; Goodrich, Mikouchi, et al., 2015; Goodrich, Ross, et al., 2017; Goodrich, Zolensky, Fioretti, et al., 2019; Goodrich, Zolensky, Kohl, et al., 2019; Ikeda et al., 2000, 2003; Jaques & Fitzgerald, 1982; Patzek et al., 2018; Prinz et al., 1986, 1987; Ross et al., 2010).

The Almahata Sitta (AhS) meteorite, which is classified as an anomalous polymict ureilite (Meteoritical Bulletin Database), fell in 2008 when the 3–4 meter-sized asteroid 2008 TC_3 shattered over northern Sudan (Jenniskens et al., 2009). The fall gave rise to a 30 km-long strewn field consisting of stones of a variety of meteorite types (Goodrich, Hartmann, et al., 2015; Horstmann & Bischoff, 2014; Jenniskens et al., 2022; Shaddad et al., 2010; Zolensky et al., 2010). Most of the recovered stones (~70%–80%) are ureilites of various types, while the remainder are chondrites including OC, EC, RC, and CC of various subgroups and types (Bischoff et al., 2022; Fioretti et al., 2017; Goodrich et al., 2018; Goodrich, Zolensky, Fioretti, et al., 2019; Hamilton et al., 2020; Horstmann & Bischoff, 2014). Initial uncertainty as to whether all these stones belonged to the same fall (e.g., Zolensky et al., 2010) was abated by studies showing that large and small stones of both ureilitic and chondritic types were of similar low weathering grade (Bischoff et al., 2010) and were found in all parts of the large strewn field (Shaddad et al., 2010), and by studies of cosmic ray exposure ages that showed agreement between ureilitic (Welten et al., 2010), EC (Bischoff et al., 2010; Riebe et al., 2017), and OC (Meier et al., 2012) stones and indicated that they were all derived from a single asteroid.

The fact that the AhS strewn field consists of stones of a large variety of meteorite types (a phenomenon never previously documented) leads to an unusual situation in the classification of this meteorite. Considering the entire collection of stones that have been studied so far, the fact that the majority of them are various types of ureilites implies that the meteorite, as a collection, is a polymict ureilite (albeit with an anomalously high fraction of non-ureilitic clasts). This does not, however, mean that any of the AhS stones are polymict ureilites. Rather, they are clasts of a variety of different lithologies, each of which has its own meteorite classification (such as OC and EC), from a polymict ureilitic breccia. In this case, the common practice of referring to individual stones from a meteorite fall as "meteorites" can be confusing, because the AhS meteorite exists only as a collection. In this paper, we refer to individual samples of AhS as stones, clasts, or fragments.

The nomenclature of AhS is additionally complicated by the fact that there are two main sources of AhS samples. The official collection of AhS samples consists of >600 stones, ~0.2–400 g in mass, which were recovered in several organized search campaigns in the predicted fall area (Shaddad et al., 2010). These samples are housed at the University of Khartoum (UoK), Sudan, and are catalogued with find coordinates that collectively define

19455100, 2024, 4, Downloaded from https://onlinelibrary.wiley.com/doi/10.1111/maps.14066 by University Of Wisconsin - Madison, Wiley Online Library on [18/06/2024]. See the Terms and Conditions (https://onlinelibrary.wiley.com/terms-and-conditions) on Wiley Online Library for rules of use; OA articles are governed by the applicable Creative Commons License

the AhS strewn field (Jenniskens et al., 2022; Shaddad et al., 2010). Independently, samples of AhS have been collected and distributed by others, without information regarding their find locations or original masses. Samples from the UoK collection are designated using the prefix AhS, with the subsequent number referring to sample numbers given in tables 1–3 of Shaddad et al. (2010). Samples of AhS from non-UoK sources have been designated with a variety of nomenclatures, most commonly MS-xxx or MS-MU-xxx (e.g., Bischoff et al., 2010, 2022; Horstmann & Bischoff, 2014).

Nature and Origin of Asteroid 2008 TC_3

The classification of asteroid 2008 TC_3, that is, the question of whether it was also a polymict ureilite, is a different matter from the classification of the meteorite. Based on the diversity of the recovered stones, it can be inferred that 2008 TC_3 was a heterogeneous breccia that disaggregated in the atmosphere. This is supported by pre-impact observations that imply that the asteroid had low density and high macroporosity and was probably only loosely consolidated (Borovička & Charvát, 2009; Jenniskens et al., 2009; Popova et al., 2011; Welten et al., 2010). These observations also imply that ≥99% of the mass of the asteroid was lost in the atmosphere, probably as fine dust (Goodrich, Hartmann, et al., 2015; Jenniskens et al., 2009, 2022; Shaddad et al., 2010). Thus, not only do the recovered stones constitute only a small fraction of the material in the asteroid, they constitute only its strongest (most coherent) clasts, and may not be representative of the bulk of the asteroid.

None of the clasts show any contacts with adhering matrix that might provide information on the composition of the lost material. The only source of such information, therefore, is the reflectance spectrum of the asteroid, which was measured in the 0.5–1 μm range shortly before impact (Jenniskens et al., 2009, 2010). The reflectance spectrum of 2008 TC_3 most closely matches F-type asteroids, which belong to the C complex of dark asteroids commonly identified with carbonaceous chondrites (DeMeo et al., 2009, 2015; Tholen & Barucci, 1989). If AhS had not been recovered, it would have been assumed that 2008 TC_3 was a carbonaceous chondrite. However, Hiroi et al. (2010) showed that spectral mixtures consisting dominantly of chips and coarse powders of various AhS ureilites (which tend to show darker, flatter spectra than main group ureilites) reproduced the main features of the asteroid's spectrum. This would suggest that 2008 TC_3 was a polymict ureilite, and may not even have been anomalous in its fraction of non-ureilitic material (Goodrich, Bottke, et al., 2021). However, Goodrich, Zolensky, Fioretti, et al. (2019) showed that the spectrum of the asteroid is also consistent with spectral mixes containing up to 70% of the carbonaceous chondrite (C1) lithology represented by AhS stone 91A (the rest being mainly ureilitic with <10% of other meteorite types), and argued that this material also provides a better match to the asteroid's density and porosity. This would suggest that 2008 TC_3 was a dominantly carbonaceous chondrite asteroid after all. Nevertheless, within the errors on the spectrum of the asteroid, these two possibilities cannot be unambiguously distinguished.

Formation of Asteroid 2008 TC_3

The fundamental question, though, is whether 2008 TC_3 (or its immediate progenitor) formed by the same processes and/or in the same environment as typical polymict ureilites. Unfortunately, even if we could determine whether 2008 TC_3 consisted dominantly of ureilitic or dominantly of carbonaceous chondritic material, it would not settle this question. For example, Goodrich, Zolensky, Fioretti, et al. (2019); Goodrich, Bottke, et al. (2021) argued that 2008 TC_3 could have been derived from a volume of regolith dominated by a single carbonaceous chondrite impactor on the same ureilitic asteroid as typical polymict ureilites. In contrast, Bischoff et al. (2022) argued that 2008 TC_3 was a polymict carbonaceous chondrite (C1) asteroid that must have formed independently from polymict ureilites. One of the main points on which this argument hinges is a comparison of the non-ureilitic clast populations in AhS versus typical polymict ureilites, focusing in particular on the relative abundances of CC and EC clasts in the two populations.

Carbonaceous chondrite (C1) clasts are the most abundant (both by number and size) foreign clasts in typical polymict ureilites (Goodrich, Sanborn, et al., 2021; Goodrich, Kring, et al., 2021), while enstatite chondrites (ECs) dominate among at least the non-UoK samples in AhS (Bischoff et al., 2022). Furthermore, until recently, CC were thought to be absent in AhS, while clasts of EC had never been reported in typical polymict ureilites. These differences have been argued to be substantial, suggesting different formation histories for 2008 TC_3 and typical polymict ureilites (Bischoff et al., 2010; Goodrich, Fioretti, et al., 2015). This partly changed with the discovery of the C1 stones AhS 91/91A and AhS 671 (Goodrich, Zolensky, Fioretti, et al., 2019) and the C2 stone AhS 202 (Hamilton et al., 2020) in the UoK collection, as well as two AhS 91A-like non-UoK samples (Bischoff et al., 2022), showing that CC do occur in AhS. However, Bischoff et al. (2022) still argued that the absence of EC in typical polymict ureilites was a "deal breaker" for a common origin. Thus, the EC in AhS are crucial for understanding the formation of 2008 TC_3, which makes it essential to determine whether EC also

19455100, 2024, 4, Downloaded from https://onlinelibrary.wiley.com/doi/10.1111/maps.14066 by University Of Wisconsin - Madison, Wiley Online Library on [18/06/2024]. See the Terms and Conditions (https://onlinelibrary.wiley.com/terms-and-conditions) on Wiley Online Library for rules of use; OA articles are governed by the applicable Creative Commons License

dominate among the non-ureilitic clasts from the UoK collection, and whether EC really are absent in typical polymict ureilites. Our work addresses both of these questions. With respect to the latter, we report the first discovery of a large EC clast in a typical polymict ureilite and use our results to argue that there are no significant differences in the types of non-ureilitic clasts in 2008 TC_3 and typical polymict ureilites.

Origin and History of Enstatite Meteorite Parent Asteroids

The EC (and related enstatite achondrite) stones from AhS are also important because they constitute fresh samples of an extremely interesting class of meteorites (Bischoff et al., 2010, 2015, 2016, 2022; El Goresy et al., 2011, 2012, 2017; Horstmann et al., 2012, 2014; Horstmann & Bischoff, 2014; Kimura et al., 2021; Weyrauch et al., 2018; Storz et al., 2021). ECs are some of the most reduced of all meteorites (Brearley & Jones, 1998; El Goresy et al., 2017; Weisberg & Kimura, 2012), containing phases in which normally lithophile elements behave as chalcophile or siderophile (such as Ca-, Mg-, and Mn-sulfides, Si-bearing metal, and Ti-Cr-bearing troilite), and thus may record an endmember in the spectrum of oxidation states in the solar nebula. They are also of interest because they show extremely similar isotope ratios to those of the Earth and Moon in many different isotope systems. This suggests a genetic affinity between ECs and the material that accreted to form the Earth (Boyet et al., 2018; Dauphas, 2017; Lodders, 2000; Sikdar & Rai, 2020), although the extent of the similarities and the degree to which they are unique is debated (e.g., Fitoussi & Bourdon, 2012; Walker et al., 2015). Ironically, the very reduced mineralogy of ECs makes them so unstable on the surface of the Earth (i.e., highly susceptible to terrestrial weathering) that the importance of having EC falls (as opposed to finds) to study cannot be overemphasized. In fact, EC falls are relatively rare—only eight EH and eight EL falls, representing only 1.6% of all meteorite falls, have been recorded (Meteorite Bulletin Database). In summarizing data for 65 AhS EC from non-UoK collections, Bischoff et al. (2022) noted that they increase the number of fresh EC in our meteorite collections by several hundred percent. These samples have been studied intensely, providing new information on mineralogical, chemical, and isotopic properties of enstatite-rich meteorites, conditions of their formation and evolution, and the number and sizes of their parent asteroids (Bischoff et al., 2010, 2022; El Goresy et al., 2017; Harries & Bischoff, 2020; Horstmann et al., 2014; Horstmann & Bischoff, 2014; Storz et al., 2021; Weyrauch et al., 2018).

At the same time, it is a nontrivial point that these stones are not actually individual meteorites. They are clasts in a breccia that were added to their host (whether a polymict ureilite or some other type of body) early in the history of the solar system, ~50–100 Myr after CAI formation (Bischoff et al., 2022; Goodrich, Sanborn, et al., 2021). Thus, they provide a snapshot of a critical stage in the collisional and dynamical evolution of enstatite meteorite parent asteroids. In this work, we evaluate whether the EC materials in AhS show any significant differences from previously known EC, and examine the implications for the origin and history of enstatite meteorite asteroids in the solar system.

Design and Objectives of this Work

In this work, we investigate the petrology and oxygen isotope compositions of enstatite meteorite samples from the UoK collection of AhS. In addition, we report the discovery of the first bona fide (multi-mm-sized) clast of an EC in a typical polymict ureilite (NWA 10657), and investigate its petrology. We use a combination of texture, mineralogy, and mineral compositions to classify these samples into subtypes using the scheme of Weyrauch et al. (2018). We then consider their oxygen isotope signatures to determine whether EC subtypes correlate with isotopic signatures.

We use our results to address the following objectives: (1) to compare the UoK enstatite meteorite samples with those from non-UoK collections of AhS to evaluate possible differences or biases between the two sources of material; (2) to evaluate the occurrences (types and relative abundances) of enstatite meteorites in asteroid 2008 TC_3 versus typical polymict ureilites to address the question of whether they formed by the same processes or in the same environment; (3) to compare the AhS enstatite meteorite clasts with the individual enstatite meteorites in our collections to evaluate whether they represent different populations of materials; and (4) to examine implications for the origin and history of enstatite meteorite asteroids in the solar system.

SAMPLES AND METHODS

All the AhS samples studied in this work are from the UoK collection (Shaddad et al., 2010). Most originate from the far southwestern end of the AhS strewn field in which the largest samples were recovered, defined as the "large mass" area by Jenniskens et al. (2009) and Shaddad et al. (2010). A total of 67 stones were found in this area, of which 66 have now been classified (Jenniskens et al., 2022). Eight of these are enstatite meteorites (seven EC and one enstatite achondrite), six of which are included in this study (AhS 17, AhS 26, AhS

19455100, 2024, 4, Downloaded from https://onlinelibrary.wiley.com/doi/10.1111/maps.14066 by University Of Wisconsin - Madison, Wiley Online Library on [18/06/2024]. See the Terms and Conditions (https://onlinelibrary.wiley.com/terms-and-conditions) on Wiley Online Library for rules of use; OA articles are governed by the applicable Creative Commons License

41, AhS 60, AhS 609, and AhS 1002). AhS 41 and another EC from the large mass area (AhS 16) were briefly described by Zolensky et al. (2010). AhS 60 was briefly described in Goodrich et al. (2018). Two other EC samples included in this study (AhS 2012 and AhS S151) were recovered outside of the large mass area. The reader is referred to Shaddad et al. (2010) and Jenniskens et al. (2022) for exact find coordinates and original masses of the samples.

Northwest Africa (NWA) 10657 is a typical polymict ureilite (Meteoritical Bulletin Database) that exhibits a moderate degree of terrestrial weathering. It contains abundant non-ureilitic clasts of a variety of types.

All samples in the UoK collection were collected free from touch in Al foil at the fall sites and were kept in a dry environment (Shaddad et al., 2010). Fragments of AhS 26, AhS 609, AhS 1002, AhS 2012, AhS S151, and AhS 60 were removed at the UoK using a Dremel power tool and metal shear press with no lubricants. These fragments were made into polished thin sections at the University of Padua, Italy, where preliminary analyses were conducted using the Cameca SX50 electron microprobe (EMP). A fragment of AhS 17 was made into a polished epoxy mount (thick section) at the Astromaterials Research and Exploration Science (ARES) division at Johnson Space Center (JSC), Houston. Sample AhS 41 was made into a polished epoxy mount (thick section) at the Natural History Museum (NHM) London. Polished thin sections NWA 10657_006 and NWA 10657_007 (adjacent serial sections) were borrowed from the XSPACE meteorite collection at LPI (XSPACE; usra.edu). All of these sections were studied in the electron beam facilities at ARES (JSC), the Department of Geosciences at the University of Massachusetts, Amherst, the Lunar and Planetary Institute (LPI), and/or the Department of Geosciences at the University of Colorado, Boulder.

Backscattered electron images (BEI) were obtained using the JEOL 8530-FE EMP at JSC, the Zeiss EVO scanning electron microscope (SEM) at the University of Massachusetts, and the Phenom XL SEM in the LPI SEM Facility. Elemental x-ray maps of whole sections of AhS 26, AhS 2012, AhS S151, and AhS 1002 were obtained using the Noran System Seven software and Bruker energy-dispersive spectrometer (EDS) on the JEOL 8530-FE at JSC operating at 15 kV and 200 nA beam current, with ~1–2 μm spatial resolution. Elemental x-ray maps of whole sections of AhS 41, AhS 17, and AhS 60 were obtained using the Cameca SXFIVE-Tactis at the University of Massachusetts. Maps were collected using a 15 kV, 200 nA, 1 μm beam by stage raster, with simultaneous collection of five elements by WDS plus hyperspectral (full spectrum per pixel) EDS. The hypermaps were then used to extract other element signals. Step (pixel) sizes were 3 μm (AhS 17), 7 μm (AhS 60), and 4 μm (AhS 41), each with a pixel dwell time of 30 ms. Elemental x-ray maps of the whole section of NWA 10657_006 were obtained using the JEOL 7600F SEM at JSC using an Oxford Ulti Max (170 mm_2 SDD type) EDS detector system with Aztec software, operating at 15 kV and 15 nA. Local area x-ray maps were obtained using the EDS system and ProSuite software on the Phenom XL SEM at LPI.

Quantitative analyses of phases by electron microprobe analysis (EMPA) were obtained using the JEOL-8530-FE at JSC, the JEOL-8200 at the University of Colorado, the Cameca SXFIVE-Tactis at the University of Massachusetts, and/or the CAMECA SX100 at the NHM. Appropriate natural and synthetic mineral, glass, and metal standards were used. ZAF matrix corrections were applied to all analyses. Pyroxene and olivine were analyzed using 15 kV, 25–30 nA beam current, and ~1 μm diameter spot size. Feldspar and silica-rich phases were analyzed using 15 kV, 10 nA beam current, and 2–5 μm diameter spot sizes. Metal and sulfides were analyzed using 15 kV, 40 nA beam current, and ~1 μm diameter spot size. Measured Co contents were corrected for overlap of the Fe K-β peak with the Co K-α peak, by analyzing Co in a pure Fe metal standard. The measured Co content in this standard was taken to be the fraction of Fe that had to be subtracted from the measured Co content for each analysis. We also evaluated the overlap of the Ti K-β peak with the V K-α peak by measuring V in a Ti standard and following a similar procedure. The correction to V contents (which were only above detection limit in troilite) was found to be insignifcant within the uncertainty of the V analyses.

Trace elements in kamacite in AhS 41 were analyzed by LA-ICP-MS at NASA JSC using a New Wave UP-193 solid-state laser ablation system attached to a Thermo Scientific Element-XR magnetic sector ICP-MS in low-resolution mode ($m/\Delta m$ = 300). Laser power was 1–2 GW cm^{-2}; repetition rate was 10 Hz; spot sizes varied from 50 to 100 μm, depending on grain size. External calibration standards were Hoba (Campbell et al., 2002; Campbell & Humayun, 1999, 2005) and Filomena (Campbell et al., 2002; Wasson et al., 1989, 1998, 2007). Corrected intensities were converted to elemental abundances by normalization to Ni content determined by EMPA. Data were processed using a spreadsheet developed by C-T Lee of Rice University, which allows for the use of multiple standards for each element.

Oxygen isotope compositions of bulk samples of AhS 1002, AhS 2012, AhS 26, AhS S151, and AhS 41 were obtained at the Open University (UK) using an infrared laser fluorination system. The sample and standards were loaded into a drilled hole in an Ni sample block and placed into a vacuum-tight chamber and heated at 70°C under vacuum for 24 h to remove any moisture. The

19455100, 2024, 4, Downloaded from https://onlinelibrary.wiley.com/doi/10.1111/maps.14066 by University Of Wisconsin - Madison, Wiley Online Library on [18/06/2024]. See the Terms and Conditions (https://onlinelibrary.wiley.com/terms-and-conditions) on Wiley Online Library for rules of use; OA articles are governed by the applicable Creative Commons License

system was flushed with BrF_5 to reduce the final blank level to <60 nmol O_2. The sample was heated in the presence of BrF_5 using a 50 W infrared CO_2 laser. The released oxygen was purified by passing it through two liquid nitrogen traps and over a bed of heater KBr. The isotopic composition of the purified oxygen was analyzed by a Thermo Fisher MAT 253 dual-inlet mass spectrometer. The precision was monitored by repeat analyses of an internal standard, and is ±0.052‰ for $\delta^{17}O$, ±0.094‰ for $\delta^{18}O$, and ±0.017‰ for $\Delta^{17}O$ (Greenwood et al., 2018).

Oxygen isotope analyses of olivine and pyroxene in AhS 60 were obtained by using a secondary ion mass spectrometer (SIMS) IMS 1280 at the University of Wisconsin-Madison. The analyses were conducted during the same session reported in Fukuda et al. (2022), using ~2 nA Cs + primary beam with 12 μm diameter. The external reproducibility of olivine running standard during the session was 0.26‰, 0.23‰, and 0.24‰ for $\delta^{18}O$, $\delta^{17}O$, and $\Delta^{17}O$, respectively, which are assigned as uncertainties of individual unknown analyses. Details of analytical conditions and instrumental bias corrections are described in Fukuda et al. (2022).

RESULTS

Petrology and Mineral Compositions

AhS Enstatite Chondrites

Figures 1–6 shows BEI and combined elemental x-ray maps of the polished sections of AhS S151, AhS 1002, AhS 2012, AhS 26, AhS 609, AhS 41, and AhS 17. The samples are fractured but have minimal terrestrial weathering effects (except for oldhamite), and contain enstatite-dominated chondrules showing various states of preservation in a matrix of enstatite, metal, sulfides, silica, albitic feldspar, and schreibersite.

AhS 1002 (Figure 2) has the largest (up to 2.2 mm in diameter) and best-defined chondrules. It also contains a prominent vein of concentrated metal (and sulfide), and a somewhat less well-defined vein consisting of fine-grained enstatite and a concentration of oldhamite. AhS S151 (Figure 1) and AhS 2012 (Figure 3a,b) both contain fairly well-defined chondrules up to ~1.25 mm diameter. AhS 26 (Figure 3c,d) has smaller chondrules, mostly <0.75 mm diameter, only a few of which are well defined. AhS 609 has mostly diffuse chondrules, with a few up to ~1 mm diameter, and is crosscut by several extensive veins of concentrated metal and sulfides (Figure 4). It is difficult to unambiguously identify any chondrules in BEI or x-ray maps of AhS 41 (Figure 5). In reflected light, poorly defined chondrules or chondrule fragments up to 0.7 mm in diameter were identified as metal-poor, near-circular regions, but much of the sample consists of euhedral enstatite crystals surrounded by and intergrown with kamacite. AhS 17 (Figure 6) has an overall equilibrated texture (coarser grained than AhS 41) consisting of intergrowths of enstatite, albitic feldspar, and metal/sulfide, but one possible, ~1.2 mm diameter, chondrule was observed (partially cut off by the edge of the section).

In all samples, enstatite is the dominant silicate mineral (Table 1). It occurs in both chondrules and matrix as euhedral laths up to 180 μm in length and also as fractured anhedral grains with tiny metal or sulfide inclusions. Enstatite (Mg# 99.1–99.8) is FeO-poor, generally with <0.5 wt% FeO, although enstatite in AhS 26 showed higher FeO contents (up to 0.68 wt%). This could be the result of the presence (observed in some places) of very small metal and/or sulfide inclusions within the enstatite grains (Brearley & Jones, 1998). MnO and Cr_2O_3 contents are mostly below detection limits (Cr is slightly higher in AhS 26, again possibly due to inclusions). Calcium contents of enstatite are higher in AhS 1002 and AhS 17 (Wo 1.0) compared with the other samples (Wo 0.1–0.3). Olivine of Fo 99 (Table 1) was observed in three chondrules in AhS 1002 (Figure 2) and in one chondrule in AhS S151 (Figure 1). Its Cr_2O_3 content is 0.06 wt% in S151 and below detection limit in AhS 1002. No high-Ca pyroxene was observed in any of the samples.

Albitic feldspars and silica occur in both chondrules and matrix. Albitic feldspars are subhedral to anhedral and up to 10 μm in length in AhS 17. They range from Ab_{80} to $Ab_{92.7}$ (Table 1), although no grains large enough to be analyzed were found in AhS S151, with AhS 17 and AhS 1002 having lower Ab contents (~80–82) than the other samples (>90). Silica (≥99% SiO_2) occurs as interstitial areas intergrown with feldspar in chondrules, and as anhedral grains up to 40 μm in size in matrix. Analyses from two of the samples showed small amounts of Al_2O_3, TiO_2, FeO, MgO, Na_2O, and K_2O (Table 1), consistent with previous studies of silica in EC (Brearley & Jones, 1998; Kimura et al., 2005). The polymorph(s) of the silica were not determined.

In addition to the metal-rich veins in AhS 1002 and AhS 609, metal grains and metal–sulfide aggregates are ubiquitous in all the samples. In AhS 1002 and AhS S151, they are roughly equant (rounded in outline) and intergrown with small silicate laths (Figures 1 and 2). In AhS 2012, AhS 26, and AhS 609, and to an even greater extent in AhS 41, metal–sulfide grains are less rounded and are intergrown with more and larger silicate laths (Figures 3–5). In AhS 17, metal areas are coarser and show a more equilibrated interstitial distribution among coarse (non-lath-shaped) enstatite grains (Figure 6). There appear to be small inclusions of graphite in some larger kamacite grains. Graphite also occurs as larger needles in AhS 2012.

19455100, 2024, 4, Downloaded from https://onlinelibrary.wiley.com/doi/10.1111/maps.14066 by University Of Wisconsin - Madison, Wiley Online Library on [18/06/2024]. See the Terms and Conditions (https://onlinelibrary.wiley.com/terms-and-conditions) on Wiley Online Library for rules of use; OA articles are governed by the applicable Creative Commons License

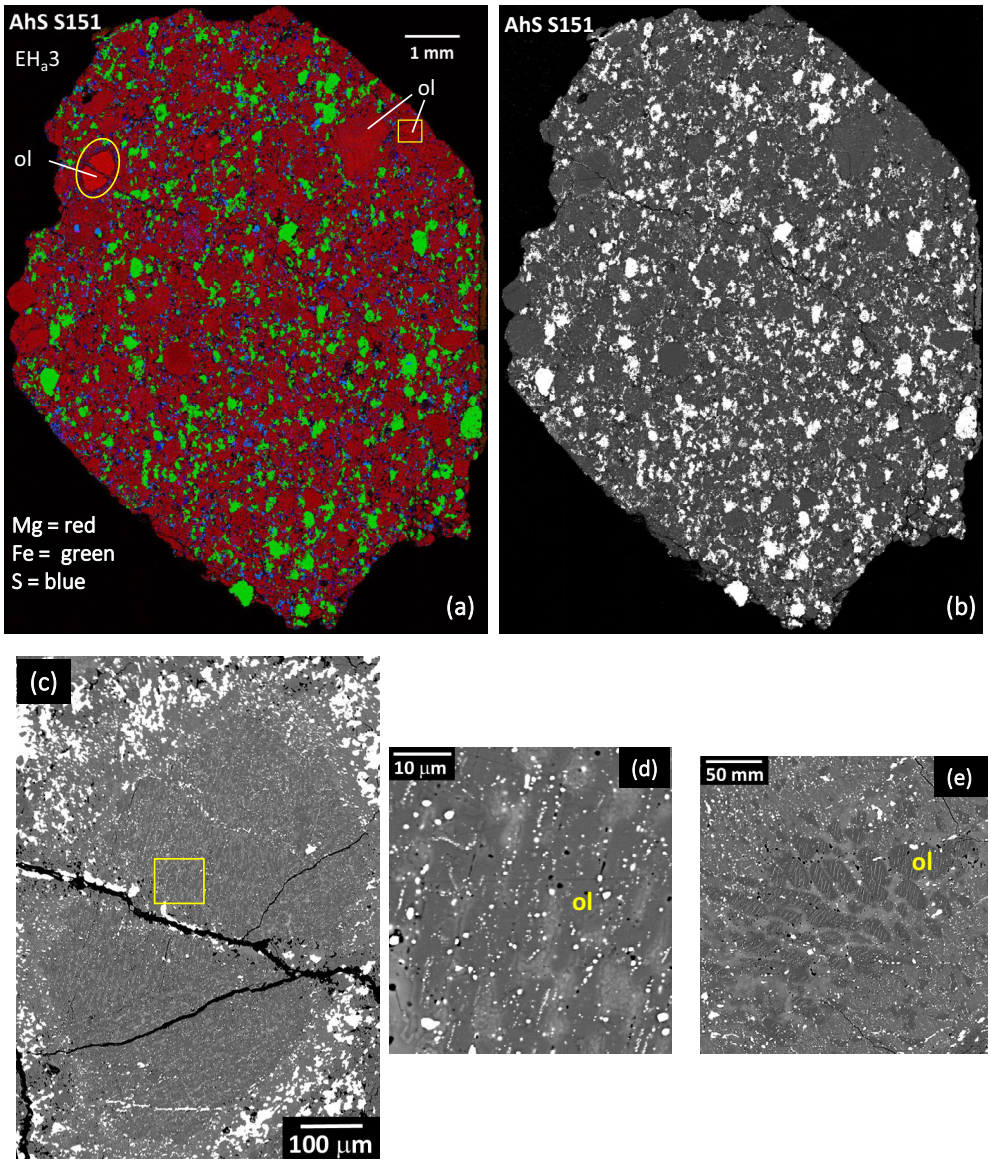

FIGURE 1. Studied section of AhS S151, classified as EH$_a$3. (a) Combined elemental x-ray map (Mg = red; Fe = green; S = blue); (b) back-scattered electron image (BEI). The main phases shown in the x-ray map are enstatite (dominant red), olivine (brighter red), metal (green), troilite (medium blue), niningerite (purplish, but not easily distinguished) and oldhamite (dark blue). (c) BEI of olivine-rich chondrule circled in upper left of (a). (d) BEI of area outlined by box in (c), showing radial olivine and mesostasis. (e) BEI of area outlined by box in upper right of (a), showing area of poikilitic olivine in a pyroxene-rich chondrule. ol, olivine. (Color figure can be viewed at wileyonlinelibrary.com)

Metal in all samples is kamacite (Table 2), with Si and Ni contents that divide them into two groups (Figure 7). AhS S151, AhS 2012, AhS 609, AhS 41, and AhS 26 show 2.4–3.1 wt% Si and 6.3–7.1 wt% Ni, plotting in the previously established field of EH metal compositions (Weyrauch et al., 2018; Zhang et al., 1995). AhS 1002 and AhS 17 show 1.1–1.5 wt% Si and 7.1–7.2 wt% Ni, plotting in the previously established field of EL metal compositions (Weyrauch et al., 2018; Zhang et al., 1995).

Siderophile element abundances in three kamacite grains from AhS 41 are given in Table 3 and plotted in Figure 8 normalized to Ni and CI chondrites (Lodders, 2003). Data for kamacite in bulk EH (Kong et al., 1997) and metal in EH impact melt rocks (Horstmann et al., 2014) are plotted for comparison. AhS 41 kamacite shows very similar abundances and patterns to previously analyzed EH metal, with As and Au above chondritic values and most of the highly siderophile elements near or slightly below chondritic values.

19455100, 2024, 4, Downloaded from https://onlinelibrary.wiley.com/doi/10.1111/maps.14066 by University Of Wisconsin - Madison, Wiley Online Library on [18/06/2024]. See the Terms and Conditions (https://onlinelibrary.wiley.com/terms-and-conditions) on Wiley Online Library for rules of use; OA articles are governed by the applicable Creative Commons License

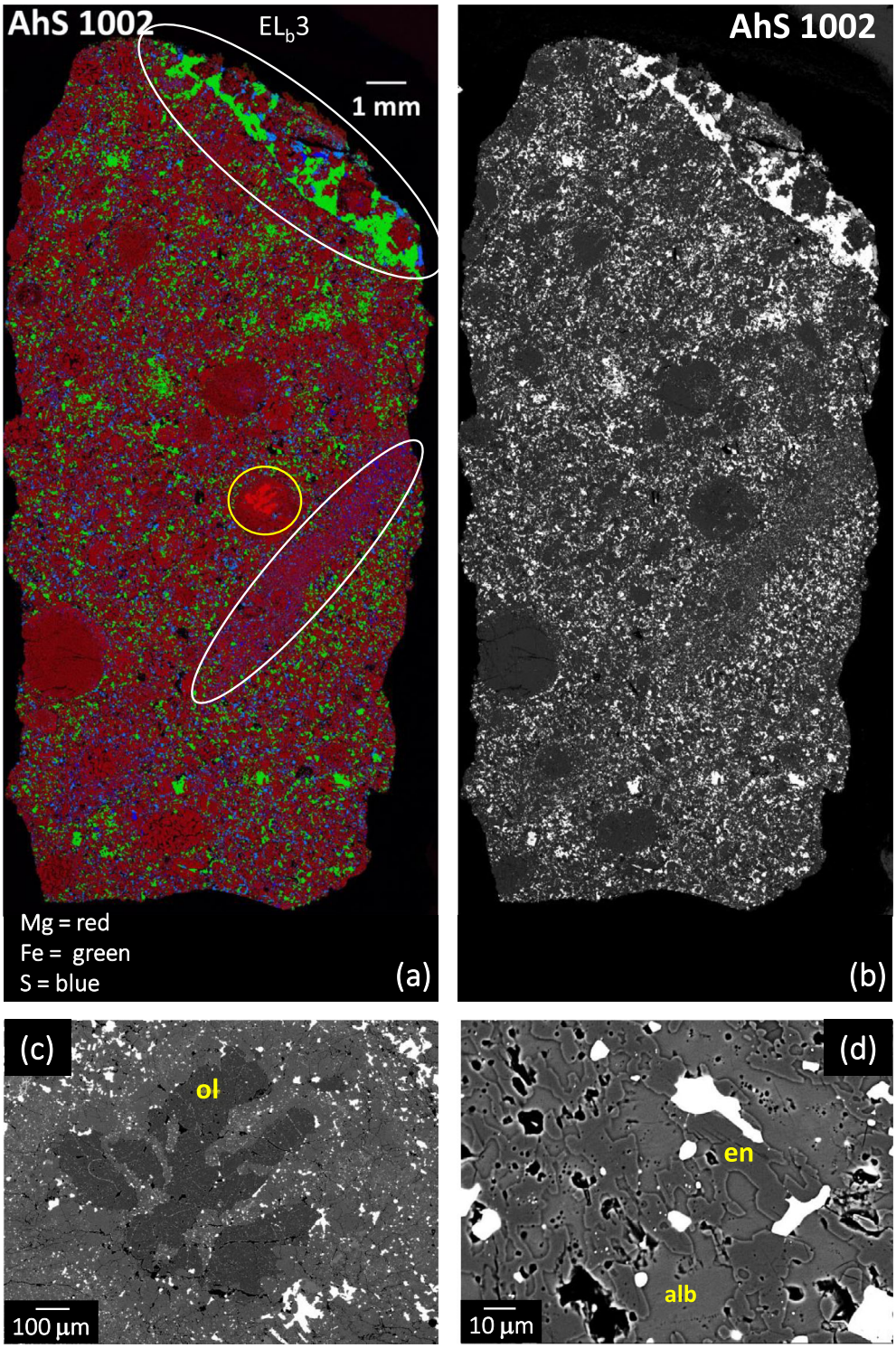

FIGURE 2. Studied section of AhS 1002, classified as EL$_b$3. (a) Combined elemental x-ray map (Mg = red; Fe = green; S = blue); (b) BEI. The main phases shown in the x-ray map are enstatite (dominant red), olivine (brighter red), metal (green), troilite (medium blue) and keilite (purplish blue, but not easily distinguished), and oldhamite (dark blue). Vein at the top of the image (circled in white) contains a concentration of metal and keilite. Vein in the middle right part of the image (also circled in white) consists of fine-grained enstatite and oldhamite. (c) BEI of olivine in chondrule circled in yellow in (a). (d) BEI showing intergrown albitic feldspar and enstatite. ol, olivine; alb, albitic feldspar; en, enstatite. (Color figure can be viewed at wileyonlinelibrary.com)

19455100, 2024, 4, Downloaded from https://onlinelibrary.wiley.com/doi/10.1111/maps.14066 by University Of Wisconsin - Madison, Wiley Online Library on [18/06/2024]. See the Terms and Conditions (https://onlinelibrary.wiley.com/terms-and-conditions) on Wiley Online Library for rules of use; OA articles are governed by the applicable Creative Commons License

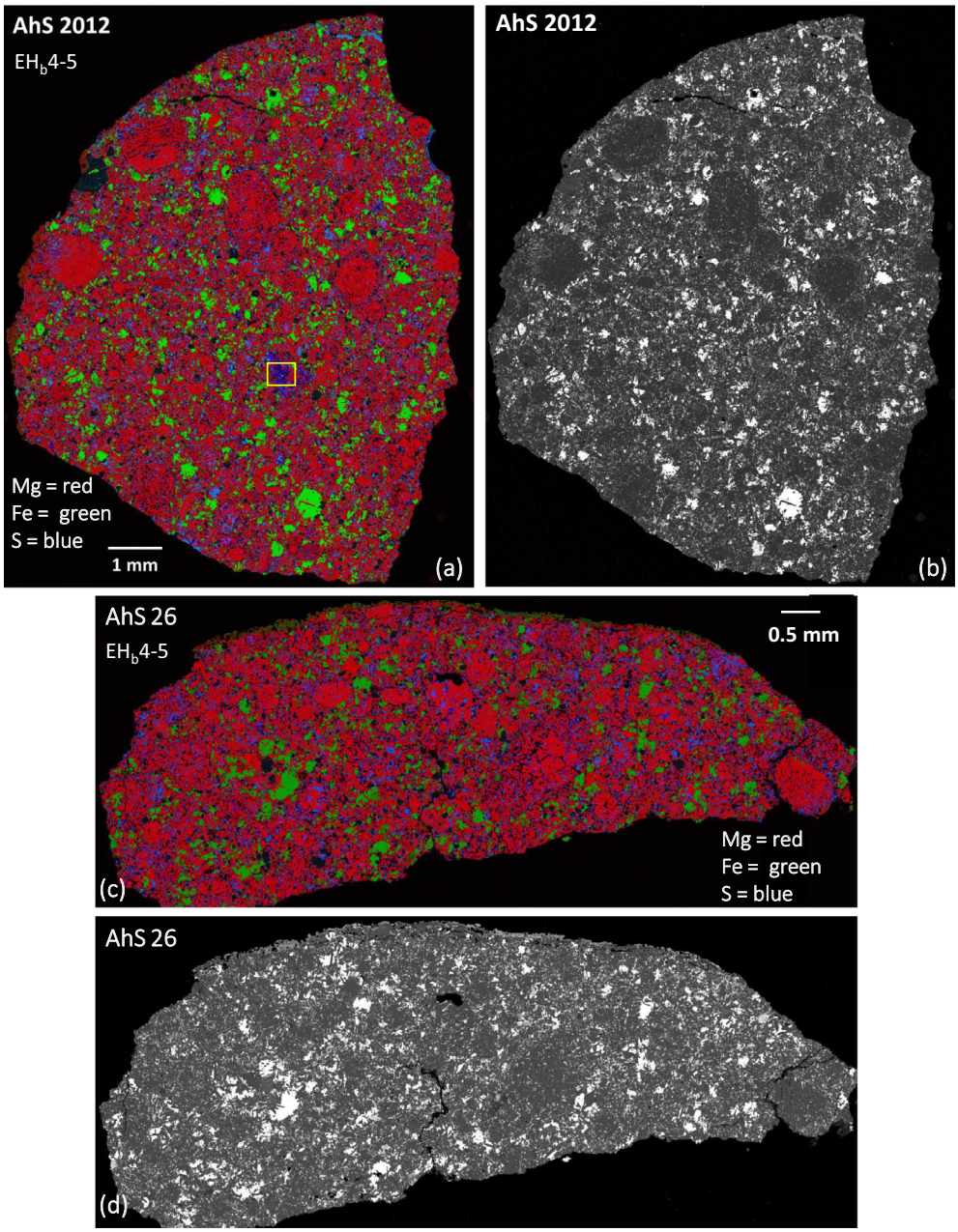

FIGURE 3. Studied sections of AhS 2012 (a, b) and AhS 26 (c, d), both classified as EH$_b$4-5. (a, c) Combined elemental x-ray maps (Mg = red; Fe = green; S = blue). (b, d) BEI. The main phases shown in the x-ray maps are enstatite (red), metal (green), troilite (medium blue), niningerite (purplish, but not easily distinguished) and oldhamite (dark blue). (Color figure can be viewed at wileyonlinelibrary.com)

The samples contain a variety of types of sulfides (Figure 9, Tables 4 and 5). Troilite is the most common sulfide in all samples. It shows Ti concentrations from ~0.4 to 0.8 wt%, and Cr concentrations of 1.1 wt% in AhS S151 and 2.6–2.9 wt% in all other samples. Mg-Mn-Fe monosulfides (as defined in Figure 10) also occur in all samples. They are niningerite in AhS S151, AhS 26, and AhS 2012 (Figure 9a,b,c,e), and keilite in AhS 609 and AhS 41 (Figure 9). Keilite also occurs in AhS 1002 and AhS 17 (Figure 9g–l), but with a more Fe- and Mn-rich composition (Figure 10). Some grains of keilite in AhS 1002 and AhS 17 contain exsolution lamellae of troilite (Figure 9h,l). Alabandite was not observed in any of the samples. Daubreelite ($FeCr_2S_4$) occurs as lamellae in troilite in AhS S151 (Figure 9e) and AhS 2012 (Figure 9c). Oldhamite (CaS) occurs in all samples (Figure 9a,c,f,i), but shows significant terrestrial weathering resulting in low EMP totals when oxygen is

19455100, 2024, 4, Downloaded from https://onlinelibrary.wiley.com/doi/10.1111/maps.14066 by University Of Wisconsin - Madison, Wiley Online Library on [18/06/2024]. See the Terms and Conditions (https://onlinelibrary.wiley.com/terms-and-conditions) on Wiley Online Library for rules of use; OA articles are governed by the applicable Creative Commons License

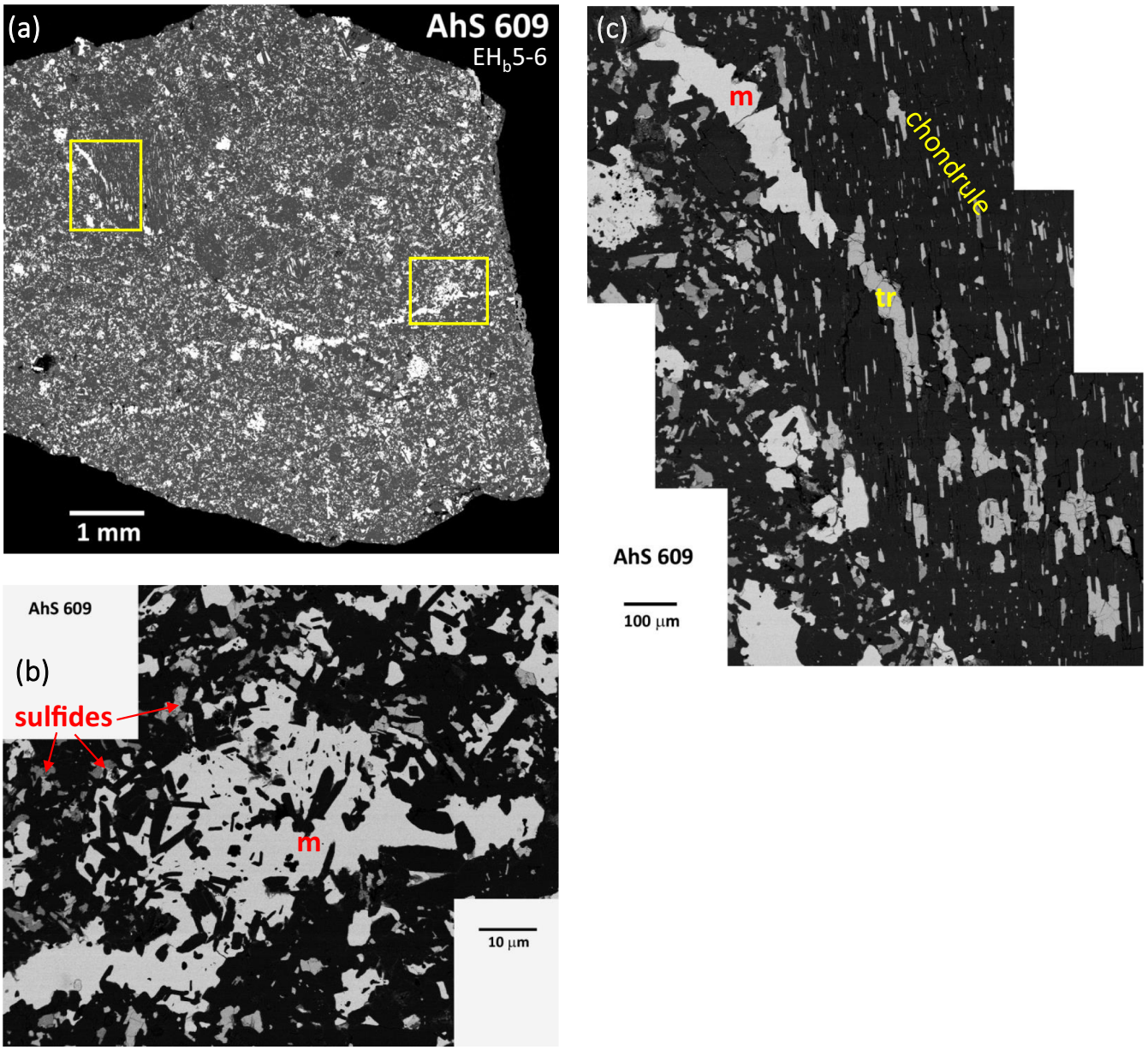

FIGURE 4. Studied section of AhS 609, classified as EH$_b$5-6. (a) BEI of most of the section. Section is cross-cut by several veins containing concentrations of metal and sulfide. (b) BEI of area of vein marked by outlined box on the right side in [a]. (c) BEI of area of vein marked by outlined box on the left side in (a). m, metal; tr, troilite. (Color figure can be viewed at wileyonlinelibrary.com)

not being measured (Table 5), as observed previously in EC (Horstmann, 2010; Weyrauch et al., 2018; Wheelock et al., 1994).

AhS 60 Enstatite Achondrite

AhS 60 is an enstatite-rich achondrite. It has an equilibrated texture with rounded, 0.5 to >3 mm-sized, grains of enstatite in a partially connected matrix of interstitial metal (Figure 11). Olivine occurs as several rounded grains, ≤1.5 mm diameter, in a cluster (Figures 11 and 12d), and also in a few irregular patches in enstatite. Modal abundances are ~75% enstatite, 3% olivine, and 22% metal.

Enstatite grains (Mg# 99.7–99.8) are not internally homogeneous (Figure 12a–c). Most of them consist dominantly of a phase with Wo 2.9–3.8 and 0.55–0.67 wt % Al_2O_3 (Table 6), but contain various abundances of irregular patches and veins of a phase with Wo ~1 and ~0.2–0.45 wt% Al_2O_3 (Table 6). The lower Wo phase contains numerous small (5–10 μm-sized) grains of high-Ca pyroxene (Figure 12b). A few highly rounded ≤1 mm-sized enstatite grains are dominated by the lower

19455100, 2024, 4, Downloaded from https://onlinelibrary.wiley.com/doi/10.1111/maps.14066 by University Of Wisconsin - Madison, Wiley Online Library on [18/06/2024]. See the Terms and Conditions (https://onlinelibrary.wiley.com/terms-and-conditions) on Wiley Online Library for rules of use; OA articles are governed by the applicable Creative Commons License

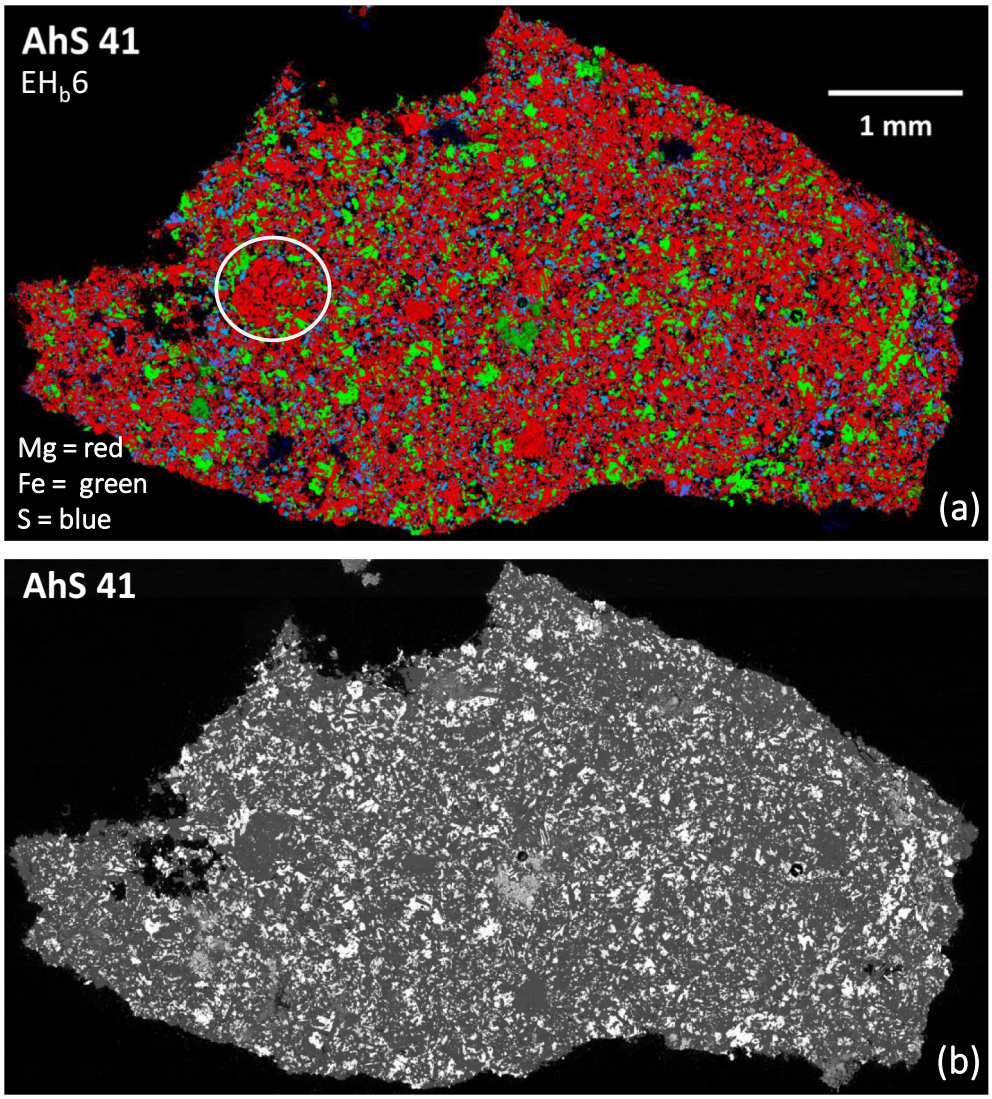

FIGURE 5. Studied section of AhS 41, classified as EH_b6. (a) Combined elemental x-ray map (Mg = red; Fe = green; S = blue); (b) BEI. The main phases shown in the x-ray map are enstatite (dominant red), olivine (brighter red), metal (green), troilite (medium blue) and keilite (purplish blue, not easily distinguished), and oldhamite (dark blue). Relict chondrules (one circled) and chondrule fragments are rare. (Color figure can be viewed at wileyonlinelibrary.com)

Wo phase, but are also not homogeneous (Figure 12a). The olivine is essentially pure forsterite with very low minor element abundances (Table 6). The metal contains 6.3 wt% Ni and 2.9 wt% Si (Table 2). No sulfides were observed.

Clast 1 (EC) in Polymict Ureilite NWA 10657_006

Clast 1 is an irregularly shaped fragment ~3.5 mm in maximum dimension (Figure 13a,b), and is the largest non-ureilitic clast in section_006 of polymict ureilite NWA 10657. A smaller fragment of what is probably the same clast occurs in section_007. Clast 1 has a chondritic texture, showing five or six well-defined chondrules ~0.6–0.75 mm in size, plus numerous smaller ones. The chondrules are porphyritic and radial pyroxene types (e.g., Figure 13c,d), dominated by enstatite (Mg# 98.6, Cr_2O_3 = 0.34 wt%, MnO = 0.12 wt%; Table 7). Two of the larger chondrules contain small, irregularly shaped grains of olivine (Fo ≥99.5) in the cores of enstatite grains (Figures 13d and 14b). The chondrules also contain interstitial silica (≥99% SiO_2) with minor amounts of FeO, Al_2O_3, and MgO (Table 7), and feldspathic mesostasis that appears from BEI and EDS to consist of fine laths of albitic feldspar in silica-rich glass (Figure 14a). One nearly spherical, ~180 μm diameter, chondrule consisting almost wholly of silica was observed (Figure 14e). Sulfides occur as interstitial grains in the chondrules mostly in minor abundances, and in some

19455100, 2024, 4, Downloaded from https://onlinelibrary.wiley.com/doi/10.1111/maps.14066 by University Of Wisconsin - Madison, Wiley Online Library on [18/06/2024]. See the Terms and Conditions (https://onlinelibrary.wiley.com/terms-and-conditions) on Wiley Online Library for rules of use; OA articles are governed by the applicable Creative Commons License

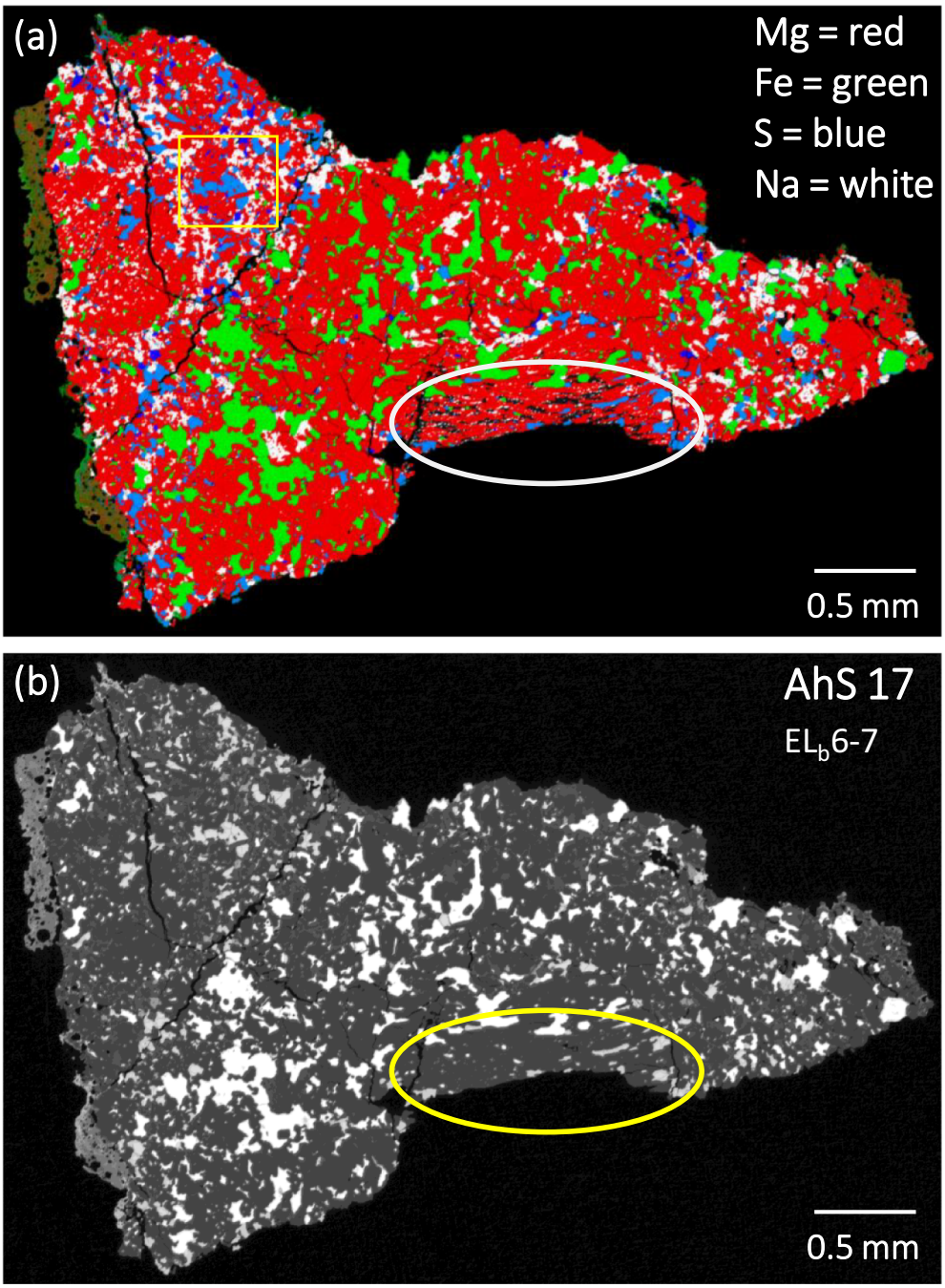

FIGURE 6. Studied section of AhS 17, classified as EL$_b$6-7. (a) Combined elemental x-ray map (Mg = red; Fe = green; S = blue; Na = white). (b) BEI. The main phases shown in the x-ray map are enstatite (red), albite (white), metal (green), troilite (medium blue), and oldhamite (dark blue). One possible relict chondrule is observed (circled, cut off by edge of section). (Color figure can be viewed at wileyonlinelibrary.com)

cases in discontinuous rims around the chondrules. The matrix of clast 1 consists of a mixture of enstatite grains of various sizes and morphologies, silica, metal, sulfides, and minor schreibersite.

Metal in clast 1 has been extensively altered to Fe-oxides, presumably by the terrestrial weathering that has affected its host NWA 10657. However, remnants of unaltered metal are found (Figure 14c,d), including in the interior of what appears to have originally been an ~300 μm diameter metal spheroid (Figures 13a,b and 14c). All analyzed metal is kamacite with average 2.8 wt % Si and 8.8 wt% Ni (Table 8). Sulfides in clast 1 have also been extensively altered to Fe-oxides (e.g., Figure 14d). The only unaltered sulfide observed (despite

19455100, 2024, 4, Downloaded from https://onlinelibrary.wiley.com/doi/10.1111/maps.14066 by University Of Wisconsin - Madison, Wiley Online Library on [18/06/2024]. See the Terms and Conditions (https://onlinelibrary.wiley.com/terms-and-conditions) on Wiley Online Library for rules of use; OA articles are governed by the applicable Creative Commons License

TABLE 1. Compositions of silicates in enstatite chondrite clasts from Almahata Sitta (AhS).

	Olivine		Pyroxene							Albitic feldspar					
Sample	AhS S151	AhS 1002	AhS S151	AhS 1002	AhS 2012	AhS 26	AhS 17	AhS 609	AhS 41	AhS 609	AhS 1002	AhS 26	AhS 2012	AhS 17	AhS 41
(#) analyses	(11)	(6)	(9)	(13)	(37)	(17)	(11)	(13)	(14)	(5)	(7)	(2)	(1)	(4)	(3)
SiO_2	42.3	42.6	59.7	59.9	60.2	60.2	59.8	60.8	60.2	70.1	66.4	70.6	69.9	65.3	68.1
TiO_2	0.18	bdl	0.01	0.01	0.01	0.01	bdl	bdl	bdl	bdl	bdl	bdl	bdl	bdl	na
Al_2O_3	1.1	bdl	0.37	0.24	0.06	0.11	0.19	bdl	0.13	18.0	20.3	18.1	18.5	20.5	18.7
Cr_2O_3	0.06	bdl	0.04	0.01	0.01	0.07	bdl	bdl	bdl	0.01	0.02	bdl	bdl	bdl	n/a
FeO	0.47	0.2	0.27	0.13	0.22	0.68	0.2	0.29	0.46	0.27	0.3	0.2	0.28	0.4	0.23
NiO	0.01	0.01	0.02	0.01	0.01	0.02	bdl	bdl	na	na	na	na	na	na	na
MgO	56.3	57.4	39.8	39.5	40.2	40.3	38.6	39.9	39.8	0.44	0.14	0.2	bdl	bdl	0.17
MnO	bdl	0.01	0.02	0.01	bdl	0.02	bdl	bdl	bdl	0.01	bdl	bdl	bdl	bdl	na
CaO	0.12	0.03	0.16	0.58	0.08	0.11	0.55	0.09	0.13	0.17	2.7	0.4	0.28	3.1	0.36
Na_2O	0.04	bdl	0.01	0.01	0.01	0.02	bdl	bdl	0.05	10.4	9.4	10.1	10.6	9.1	10.6
K_2O										1.1	0.81	1.3	1.0	0.85	0.98
Total	100.6	100.2	100.4	100.4	100.8	101.5	99.3	101.1	100.8	100.4	100.2	101.0	100.7	99.4	99.1
Fo/Mg#	99.5	99.8	99.6	99.8	99.7	99.1	99.7	99.6	99.4						
Wo			0.29	1.0	0.15	0.19	1.0	0.16	0.23						
En			99.3	98.8	99.6	98.9	98.7	99.4	99.1						
Ab										92.7	82.3	90.4	92.9	80.0	92.6
Or										6.5	4.7	7.7	5.8	4.9	5.7

	Silica phase	
Sample	AhS 41	AhS 609
(#) analyses	(3)	(1)
SiO_2	99.6	98.8
TiO_2	bdl	0.5
Al_2O_3	0.54	bdl
Cr_2O_3	na	0.29
FeO	0.52	bdl
NiO	na	bdl
MgO	0.07	bdl
MnO	bdl	bdl
CaO	bdl	0.4
Na_2O	0.28	0.05
K_2O	0.06	na
Total	101.0	100.0
Fo/Mg#		
Wo		
En		
Ab		
Or		

Note: Fo/Mg# = 100 × molar Mg/(Mg + Fe); En = 100 × molar Mg/(Mg + Fe + Ca); Wo = 100 × molar Ca/(Mg + Fe + Ca); Ab = 100 × molar Na/(Na + Ca + K); Or = 100 × molar K/(Na + Ca = K).
Abbreviations: bdl, below detection limit; na, not analyzed.

an extensive search for other types) was troilite, with 1.8 wt% Cr (Table 8).

In addition, both chondrules and matrix in clast 1 contain irregular patches and veins of a silicate phase (Figure 13c,d, circled) that does not correspond to any mineral (~72 wt% SiO_2, 20 wt% MgO; Table 7) and which we interpret to be shock melt.

Oxygen Isotopes

The oxygen isotope results for the four analyzed bulk EC clasts are given in Table 9 and plotted on the $\delta^{18}O$ versus $\Delta^{17}O$ diagram in Figure 15. All samples have $\Delta^{17}O$ values within the range of previously analyzed EC (Newton et al., 2000), and AhS EC clasts from non-UoK

19455100, 2024, 4, Downloaded from https://onlinelibrary.wiley.com/doi/10.1111/maps.14066 by University Of Wisconsin - Madison, Wiley Online Library on [18/06/2024]. See the Terms and Conditions (https://onlinelibrary.wiley.com/terms-and-conditions) on Wiley Online Library for rules of use; OA articles are governed by the applicable Creative Commons License

TABLE 2. Compositions of metal in enstatite chondrite and achondrite clasts from Almahata Sitta (AhS).

	EH					EL		
(#) analyses	AhS S151 (15)	AhS 2012 (20)	AhS 609 (35)	AhS 41 (23)	AhS 26 (7)	AhS 1002 (12)	AhS 17 (31)	AhS 60 (60)
P	0.06	0.15	0.22	0.24	0.14	0.53	0.45	0.04
S	bdl	bdl	bdl	bdl	bdl	bdl	bdl	bdl
Si	3.1	2.5	2.4	2.5	2.5	1.5	1.1	2.9
Fe	90.4	90.8	89.8	89.4	91.5	90.0	90.0	91.1
Ni	6.3	6.6	7.1	7.1	6.5	7.2	7.1	6.3
Cr	0.01	0.01	bdl	0.03	0.01	0.01	0.02	0.16
Co	0.34	0.33	0.31	0.34	0.34	0.35	0.32	0.35
Total	100.4	100.6	99.9	99.6	101.1	99.7	99.0	100.9

Abbreviation: bdl, below detection limit.

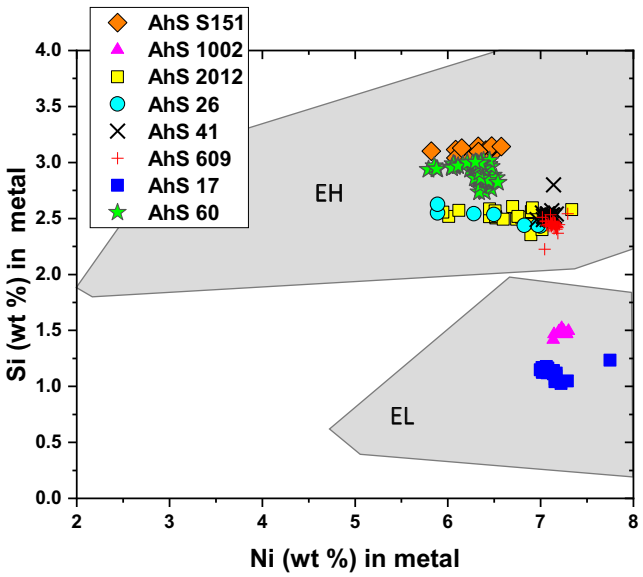

FIGURE 7. Ni and Si abundances in kamacite in the AhS clasts studied in this work. Fields for kamacite in EH and EL chondrites from Zhang et al. (1995). (Color figure can be viewed at wileyonlinelibrary.com)

collections (Horstmann & Bischoff, 2014). Three of them (AhS 1002, AhS 2012, and AhS 28) plot very close to the terrestrial fractionation line with $\Delta^{17}O$ values in the range −0.005‰ to 0.029‰, while AhS S151 has a significantly lower $\Delta^{17}O$ value of −0.29‰.

The results of 12 SIMS oxygen isotope analyses of olivine and pyroxene in the AhS 60 enstatite achondrite are given in Table 10 (see Table S1 for raw data, and Figure S1 for images of analysis spots). All analyses are indistinguishable within analytical uncertainties. The mean of all olivine and pyroxene analyses (Table 10; Figure 15) shows $\delta^{18}O = 5.61 \pm 0.32‰$ and $\delta^{17}O = 3.09 \pm 0.18‰$ ($\Delta^{17}O = 0.18 \pm 0.10‰$), which is within the range of EC but shows distinctly higher $\Delta^{17}O$ than aubrites (Barrat et al., 2016; Newton et al., 2000).

TABLE 3. Abundances of highly siderophile elements (HSE) in metal in AhS 41 in parts per million (ppm).

Spot size (μm)		M7 50	M1 100	M9 75
Fe	Fe57	895,315	925,463	890,239
Co	Co59	3407	3368	3327
Ni	Ni60	70,900	71,300	70,400
Cu	Cu63/Cu65	398	335	417
Ga	Ga69	57.2	49.9	64.2
Ge	Ge72/Ge74	135.5	127.8	149.1
As	As75	19.7	21.3	21.8
Mo	Mo95	2.79	5.65	3.56
Ru	Ru101	3.11	3.23	2.86
Rh	Rh103	0.779	0.773	0.766
Pd	Pd105/Pd106	3.12	3.09	3.02
W	W182	0.515	0.491	0.487
Re	Re185	0.230	0.171	0.230
Os	Os192	2.48	1.78	2.25
Ir	Ir193	2.36	1.79	2.03
Pt	Pt194/Pt195	4.22	3.40	3.58
Au	Au197	1.80	1.46	1.47

DISCUSSION

Classification of EC Clasts

The petrologic and mineral compositional characteristics of the EC clasts studied here can be used to classify them into subgroups (Table 11), following the scheme of Weyrauch et al. (2018). They are first divided into EL (AhS 1002, AhS 17) and EH (AhS S151, AhS 2012, AhS 26, AhS 41, AhS 609, and clast 1) types based on Si content of kamacite (Zhang et al., 1995), as shown in Figure 7. The slightly higher CaO contents of enstatite and lower Na_2O contents of albitic feldspar (compared with the other samples) in AhS 1002 and AhS 17 are consistent with this classification (Brearley & Jones, 1998). The samples are further subdivided into "a" and

19455100, 2024, 4, Downloaded from https://onlinelibrary.wiley.com/doi/10.1111/maps.14066 by University Of Wisconsin - Madison, Wiley Online Library on [18/06/2024]. See the Terms and Conditions (https://onlinelibrary.wiley.com/terms-and-conditions) on Wiley Online Library for rules of use; OA articles are governed by the applicable Creative Commons License

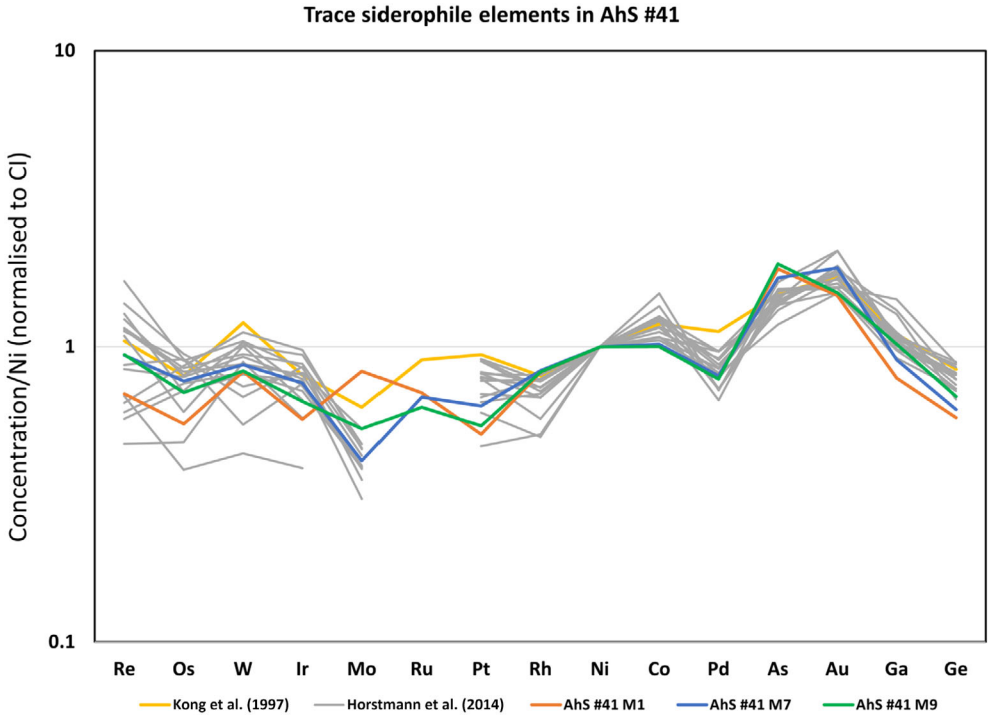

FIGURE 8. Highly siderophile elements (in order of increasing volatility) in kamacite grains analyzed by LA-ICP-MS in AhS 41, normalized to Ni and CI chondrites (Lodders, 2003). Shown for comparison are bulk EH metal (analyzed by INAA) from Kong et al. (1997), and metal grains analyzed by LA-ICP-MS in EH impact melts from Horstmann et al. (2014). (Color figure can be viewed at wileyonlinelibrary.com)

"b" types based on Cr content in troilite (<2 wt% in "a" and >2 wt% in "b"), Fe content in Fe-Mn-Mg sulfides (<20 wt% in "a" and >20 wt% in "b"; Figure 10), and Mn content of Fe-Mn-Mg sulfides (Figure 10) following Weyrauch et al. (2018). Petrologic types are first assigned based on mineralogy—specifically, the occurrence of olivine in AhS 1002 and AhS S151 implies that they are type 3 (Bendersky et al., 2007; Nehru et al., 1984; Prinz et al., 1985; Weyrauch et al., 2018). The low Cr_2O_3 contents of olivine (≤0.06 wt%) in these samples (Table 1) suggest petrologic subtype >3.2 (Bendersky et al., 2007). The other samples are classified as higher petrologic types based on textural criteria, that is, how well chondrules are delineated from matrix, as well as the shapes and sizes of metal/sulfide grains and the degree to which they are intergrown with silicates (Weyrauch et al., 2018). Specifically, chondrules become increasingly difficult to recognize, while metal/sulfide grains become increasingly irregular in shape and intergrown with enstatite laths, in the sequence AhS 2012 and AhS 26 (type 4–5) → AhS 609 (type 5–6) → AhS 41 (type 6) → AhS 17 (type 6–7).

Summarizing these classification criteria, the seven AhS EC that we studied comprise one EH_a3 (S151), one EL_b3 (AhS 1002), two EH_b4-5 (AhS 2012, AhS 26), two EH_b5-6 or possibly impact melt rocks (AhS 609, AhS 41), and one EL_b6-7 (AhS 17). Keil (2007) argued that keilite in EC formed from pre-existing niningerite or alabandite at elevated temperatures during impact melting and quenching. This is consistent with classification of AhS 609, AhS 41, and AhS 17 as high petrologic types. However, the presence of keilite in AhS 1002 is puzzling, as this sample is petrologic type 3 and does not appear to have been impact melted. Some of the keilite in this sample shows exsolution lamellae of troilite, which Keil (2007) suggested was due to slow cooling during burial following impact melting. However, the preservation of olivine, sharp chondrule outlines, and the metal/sulfide textures in AhS 1002 are not consistent with melting and re-equilibration. In fact, Weyrauch et al. (2018) identified all EL_b ECs (which AhS 1002 and AhS 17 both are) as containing keilite (Figure 10), and yet these include the entire range of petrologic types from 3 to 6. This suggests that the presence of keilite as a universal indicator of impact melting should be reconsidered.

Based on its petrologic and mineral compositional properties, clast 1 from NWA 10657_006 is an EC and can also be classified by subtype (Table 11), despite effects of terrestrial weathering and small amounts of impact melt that obscure some of its features. Based on the Si content of its metal, the Cr content of its troilite, the presence of olivine, and its well-delineated chondrules, it is EH_a3. The Cr_2O_3 content of olivine suggests petrologic subtype ~3.2 (Bendersky et al., 2007).

19455100, 2024, 4, Downloaded from https://onlinelibrary.wiley.com/doi/10.1111/maps.14066 by University Of Wisconsin - Madison, Wiley Online Library on [18/06/2024]. See the Terms and Conditions (https://onlinelibrary.wiley.com/terms-and-conditions) on Wiley Online Library for rules of use; OA articles are governed by the applicable Creative Commons License

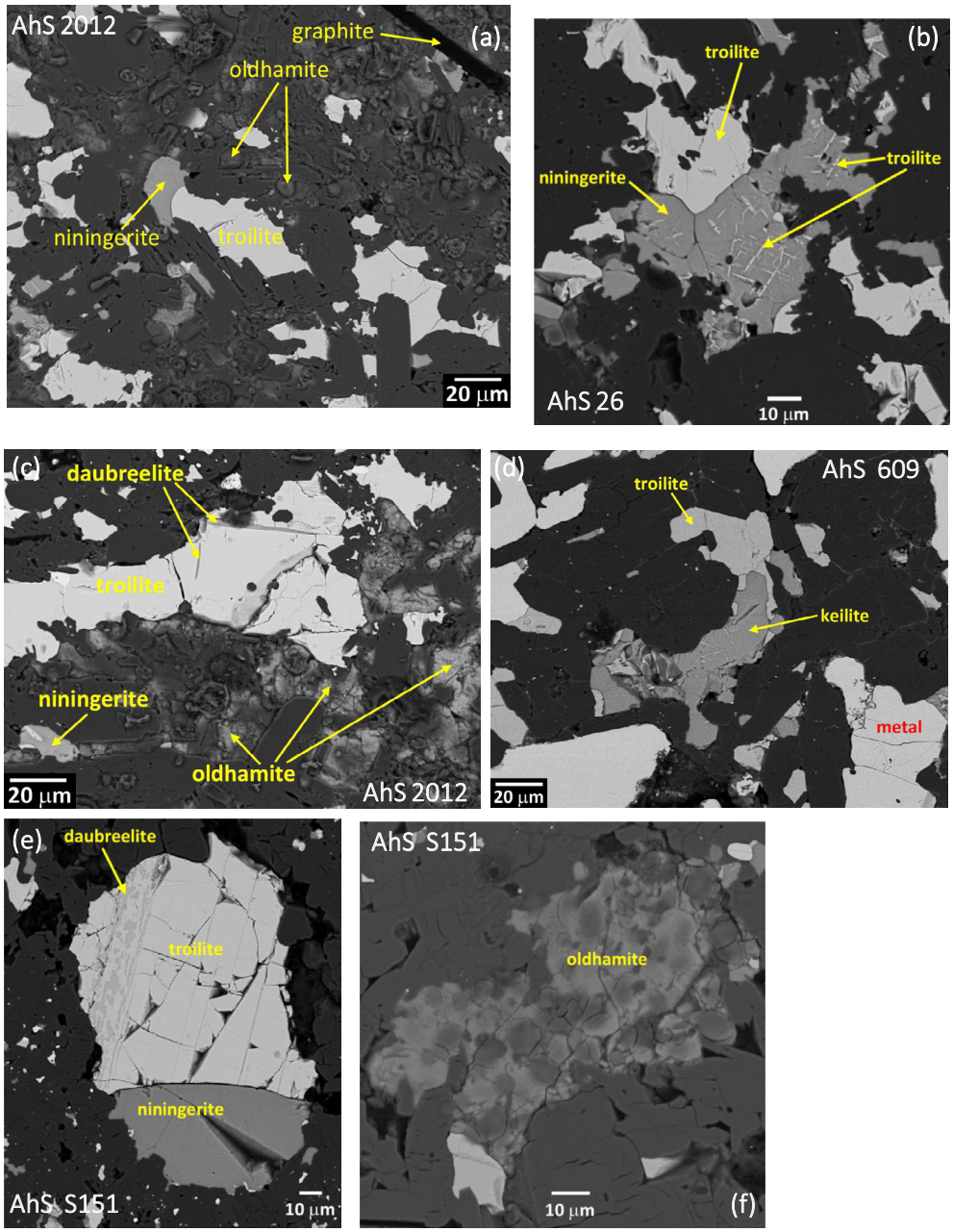

FIGURE 9. Sulfide assemblages in AhS EC. All images except [i] are BEI. (a) Troilite, niningerite and oldhamite in AhS 2012, from area outlined by box in Figure 3a. (b) Troilite and niningerite (with troilite exsolution lamellae) in AhS 26. (c) Troilite (with exsolution lamellae of daubreelite), niningerite, and oldhamite in AhS 2012. (d) Troilite, keilite, and metal in AhS 609. (e) Troilite (with exsolved daubreelite) and niningerite in AhS S151. (f) Weathered oldhamite in AhS S151. (g) Troilite and keillite in AhS 1002. (h) Keilite (with exsolved troilite) and metal in metal-rich vein (upper circled area of Figure 2a) in AhS 1002. (i) Combined x-ray map (Fe = red; Na = yellow; Ca = green; S = blue) of AhS 17 (area outlined by box in Figure 6a). Troilite contains narrow lamellae (dark blue) of keilite. alb = albitic feldspar. (j) Troilite, with keilite and metal in AhS 17. (k) BEI of area of AhS 17 outlined by box in [i] showing troilite with rim of keilite. (l) BEI of grain of troilite with patches of keilite in AhS 17. Keilite contains lamellae of troilite. (Color figure can be viewed at wileyonlinelibrary.com)

Comparison of AhS Enstatite Meteorites From the UoK and Non-UoK Collections

Bischoff et al. (2022) summarized data for 65 non-UoK AhS EC described in a number of papers (Bischoff et al., 2010; El Goresy et al., 2017; Horstmann & Bischoff, 2014; Horstmann et al., 2014; Weyrauch et al., 2018; Storz et al., 2021), as well as many abstracts and theses (see Bischoff et al., 2022 for references). These clasts comprise a large range of types including EH_a

19455100, 2024, 4, Downloaded from https://onlinelibrary.wiley.com/doi/10.1111/maps.14066 by University Of Wisconsin - Madison, Wiley Online Library on [18/06/2024]. See the Terms and Conditions (https://onlinelibrary.wiley.com/terms-and-conditions) on Wiley Online Library for rules of use; OA articles are governed by the applicable Creative Commons License

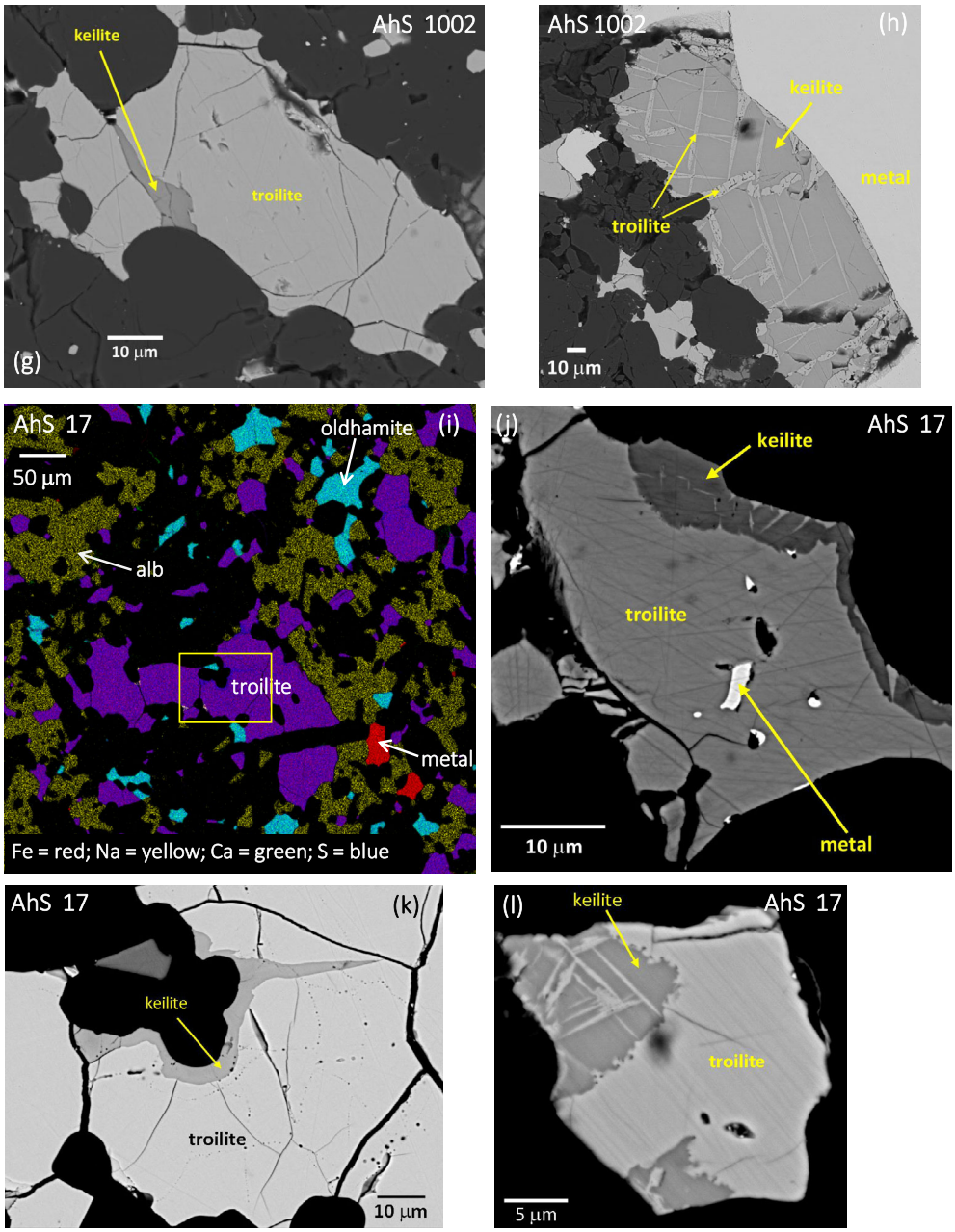

FIGURE 9. Continued

(~14%), EH_b (~20%), EL_a (~6%), and EL_b (~60%) of petrologic types 3–6 and impact melt rocks, and also include one breccia (EL of mixed petrologic types). Overall, 66% of them are EL and 34% are EH, while 80% are type "b" and 20% are type "a".

Based on our results, the EC clasts from the UoK collection show the same large range of types (except for breccias) as the non-UoK samples. They show a similar proportion of type "b" (85%) compared to type "a," but a lower proportion of EL to EH (38% EL). Considering the smaller number of UoK samples, the difference in proportion of EL to EH may not be significant. It is clear, however, that the two sources of AhS EC samples show the same large range of petrologic and compositional types, and, indeed, have very similar petrologic, chemical, and oxygen isotopic compositions. In fact, from comparing our data with images and descriptions in Weyrauch et al. (2018) and Bischoff et al. (2022), we propose very close resemblances (possible identities) between AhS 17 and MS-052 (EL_b6), AhS 2012/26 and MS-013 (EH_b5), AhS 1002/S151 and MS-MU-031 (EL_a3), and AhS 41 and MS-MU-039 (impact melt rock).

19455100, 2024, 4, Downloaded from https://onlinelibrary.wiley.com/doi/10.1111/maps.14066 by University Of Wisconsin - Madison, Wiley Online Library on [18/06/2024]. See the Terms and Conditions (https://onlinelibrary.wiley.com/terms-and-conditions) on Wiley Online Library for rules of use; OA articles are governed by the applicable Creative Commons License

TABLE 4. Types of sulfides present in enstatite chondrite clasts from Almahata Sitta (AhS).

	EH					EL	
	AhS S151	AhS 2012	AhS 609	AhS 41	AhS 26	AhS 17	AhS 1002
Niningerite	Yes	Yes			Yes		
Keilite			Yes	Yes		Yes	Yes
Troilite	Yes	Yes	Yes	Yes	Yes	Yes	Yes
Alabandite						In troilite	In troilite
Oldhamite	Yes	Yes	Yes	Yes	Yes	Yes	Yes
Daubreelite	In troilite	In troilite					

TABLE 5. Compositions of sulfides in enstatite chondrite clasts from Almahata Sitta (AhS).

	AhS S151			AhS 2012			AhS 1002			
	Troilite	Niningerite	Oldhamite	Troilite	Niningerite	Oldhamite	Troilite	Oldhamite	Keilite	Troilite lamellae in keilite
(#) analyses	(8)	(15)	(12)	(6)	(6)	(3)	(12)	(6)	(3)	(2)
P	bdl	bdl	bdl	bdl	bdl	bdl	bdl	bdl	bdl	bdl
S	37.1	47.3	40.5	37.2	44.0	42.2	37.1	41.9	39.4	37.0
Ca	bdl	1.1	52.2	0.06	1.7	53.0	bdl	51.7	2.4	0.31
Si	bdl	0.08	0.05	0.12	0.05	0.06	bdl	bdl	bdl	bdl
Mg	0.01	24.6	1.5	0.17	16.5	1.1	0.1	1.1	5.5	0.06
Fe	59.9	18.1	0.61	57.3	26.6	0.51	57.3	1.02	38.2	58.3
Ni	0.03	0.01	0.02	0.11	bdl	bdl	0.18	0.01	0.02	0.07
Cr	1.1	0.56	0.02	2.9	1.7	0.01	2.8	0.03	1.5	2.1
Co	bdl	bdl	bdl	bdl	bdl	bdl	bdl	bdl	bdl	bdl
Mn	0.04	7.81	0.39	0.15	7.25	0.36	1.04	1.31	11.4	0.72
Ti	0.78	0.01	bdl	0.62	0.04	bdl	0.42	bdl	0.03	0.07
V	0.09	0.01	bdl	0.08	bdl	bdl	0.05	bdl	bdl	bdl
Total	99.1	99.7	95.3	98.8	97.9	97.2	99.0	97.1	98.5	98.7

	AhS 26			AhS 41			AhS 609		AhS 17	
(#) analyses	Troilite (2)	Oldhamite (3)	Niningerite (6)	Troilite (20)	Keilite (5)	Oldhamite (7)	Troilite (25)	Keilite (24)	Troilite (31)	Keilite (5)
P	bdl	bdl	bdl	bdl	bdl	bdl	bdl	na	bdl	bdl
S	37.6	41.1	44.3	37.1	42.4	41.3	37.6	43.4	38.2	39.3
Ca	bdl	53.5	1.3	0.04	2.4	49.5	bdl	2.3	bdl	0.67
Si	0.03	0.04	0.04	0.1	0.02	0.12	bdl	bdl	bdl	0.07
Mg	0.09	1.0	17.0	0.06	11.1	1.5	na	11.5	n/a	4.8
Fe	57.7	0.49	26.1	58.6	35.8	2.4	59.2	36.1	56.9	38.1
Ni	0.12	0.01	0.01	0.03	bdl	0.07	0.05	0.03	0.17	0.04
Cr	2.6	0.01	1.9	2.7	1.8	0.04	2.6	1.7	3.1	1.4
Co	bdl	bdl	bdl	bdl	bdl	bdl	bdl	bdl	bdl	0.06
Mn	0.27	0.32	7.8	0.26	4.9	0.40	0.23	5.0	1.0	14.5
Ti	0.46	bdl	0.05	0.46	0.07	bdl	0.40	0.05	0.49	0.08
V	0.06	bdl	bdl	na	bdl	na	na	na	na	0.02
Total	98.9	96.5	98.5	99.3	98.3	95.2	100.1	100.7	99.9	99.1

Note: Detection limits for minor elements in wt%: P—0.003; Ca—0.008; Si—0.007; Mg—0.003; Ni—0.016; Cr—0.008; Co—0.01; Mn—0.008; Ti—0.009; V—0.008.
Abbreviations: bdl, below detection limit; na, not analyzed.

The overall similarities between the UoK and the non-UoK AhS enstatite meteorites are further supported by our recognition of AhS 60 among the UoK samples. AhS 60 is an enstatite-dominated achondrite that differs in texture, mineralogy (e.g., absence of plagioclase, virtual absence of sulfides), and oxygen isotope

19455100, 2024, 4, Downloaded from https://onlinelibrary.wiley.com/doi/10.1111/maps.14066 by University Of Wisconsin - Madison, Wiley Online Library on [18/06/2024]. See the Terms and Conditions (https://onlinelibrary.wiley.com/terms-and-conditions) on Wiley Online Library for rules of use; OA articles are governed by the applicable Creative Commons License

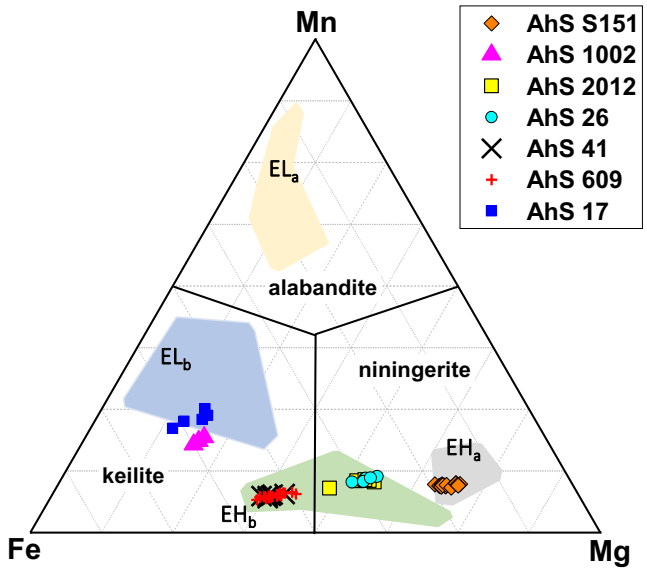

FIGURE 10. Ternary diagram for cubic Fe-Mn-Mg sulfides (field for keilite as defined in Shimizu et al., 2002), showing compositions for the AhS EC clasts studied in this work. Fields for sulfides in EH_a, EH_b, EL_a, and EL_b plotted from the data in Weyrauch et al. (2018). (Color figure can be viewed at wileyonlinelibrary.com)

compositions (Figure 15) from aubrites (e.g., Brearley and Prinz 1998), as well as from other unique enstatite achondrites such as Shallowater (Keil et al., 1989), Itqiy (Patzer et al., 2001), and NWA 2525 (Keil & Bischoff, 2008). It is virtually identical in mineralogy, texture, and mineral compositions to the non-UoK AhS clasts MS-MU-019 and MS-MU-036 described by Harries and Bischoff (2020). The occurrence of this unique enstatite meteorite lithology among both the UoK and non-UoK AhS stones strongly supports the conclusion that there are no significant differences in the range of sample types between these different sources of AhS material.

Implications for the Formation of Asteroid 2008 TC_3

Enstatite Meteorite Clast Populations in AhS and Typical Polymict Ureilites

Enstatite chondrites were reported to be the most abundant non-ureilitic clasts in AhS, based on samples from non-UoK collections (Bischoff et al., 2010, 2022; Horstmann & Bischoff, 2014). In a compilation of data for 249 non-UoK AhS stones, Bischoff et al. (2022) report that 65 of the 81 non-ureilites (80%) are EC. One of the goals of this work was to determine whether EC are also the most abundant non-ureilites among the UoK stones. Combining our results with the classifications reported in Jenniskens et al. (2022) and Zolensky et al. (2010), we find that 78% of the non-ureilites from the "large mass" area of the AhS strewn field (Shaddad et al., 2010) are EC, which is similar to the non-UoK collections.

In contrast, enstatite meteorite material is rare in typical polymict ureilites (TPUs). Goodrich, Fioretti, et al. (2015) made a targeted search for such material in sections of six polymict ureilites and found that enstatite grains having major and minor element compositions and mineral inclusions consistent with derivation from ECs or aubrites were present, but only in very low abundance. Downes et al. (2008) reported one enstatite grain having oxygen isotope composition consistent with EC from a study of six sections of polymict ureilites. Boleaga and Goodrich (2019) surveyed metal in two sections of polymict ureilites and found that half the non-ureilitic metal grains had compositions distinguishing them as EC-like (both EH and EL). Despite these indications that some enstatite meteorite material is present in polymict ureilites, lithic clasts of EC (or even isolated chondrules unambiguously derived from them) or enstatite achondrites had not been reported before this work. Bischoff et al. (2022) wrote that "the lack of millimeter- to centimeter-sized E chondrite fragments in (typical) polymict ureilites. . ..clearly speaks against a common origin of polymict ureilites and 2008 TC_3-like materials." Our discovery of a 3.5 mm-sized EC (EH_a3) clast in a typical polymict ureilite certainly decimates this argument.

Given this discovery, it now seems likely that there are no major differences in the range of types of non-ureilitic materials in AhS and TPUs. We argue in the following section that this strongly suggests a common origin for AhS and TPUs. There may be differences in the relative abundances of different types of materials, for example, the EC, but such differences might be expected in the model that we propose. Furthermore, it is possible that the difference in abundance of EC is less than it seems, since EC clasts in 2008 TC_3 may have preferentially survived atmospheric entry due to their greater strength relative to other types of materials.

Formation of AhS and Typical Polymict Ureilites in the Same Regolith Environment

All scenarios that have been proposed for formation of TPUs begin with the catastrophic disruption of the UPB at ~5–5.4 Myr after CAI (Downes et al., 2008; Goodrich, Hartmann, et al., 2015; Goodrich, Kring, et al., 2021; Goodrich, Sanborn, et al., 2021; Goodrich et al., 2004, 2010; Herrin et al., 2010). This event was immediately followed by gravitational re-accumulation of subsets of the dispersed fragments to form daughter bodies, each of which was made of a different mixture of jumbled materials from disparate parts of the UPB (Michel et al., 2001, 2015). Thus, the observation that polymict ureilites show the same range and characteristic

19455100, 2024, 4, Downloaded from https://onlinelibrary.wiley.com/doi/10.1111/maps.14066 by University Of Wisconsin - Madison, Wiley Online Library on [18/06/2024]. See the Terms and Conditions (https://onlinelibrary.wiley.com/terms-and-conditions) on Wiley Online Library for rules of use; OA articles are governed by the applicable Creative Commons License

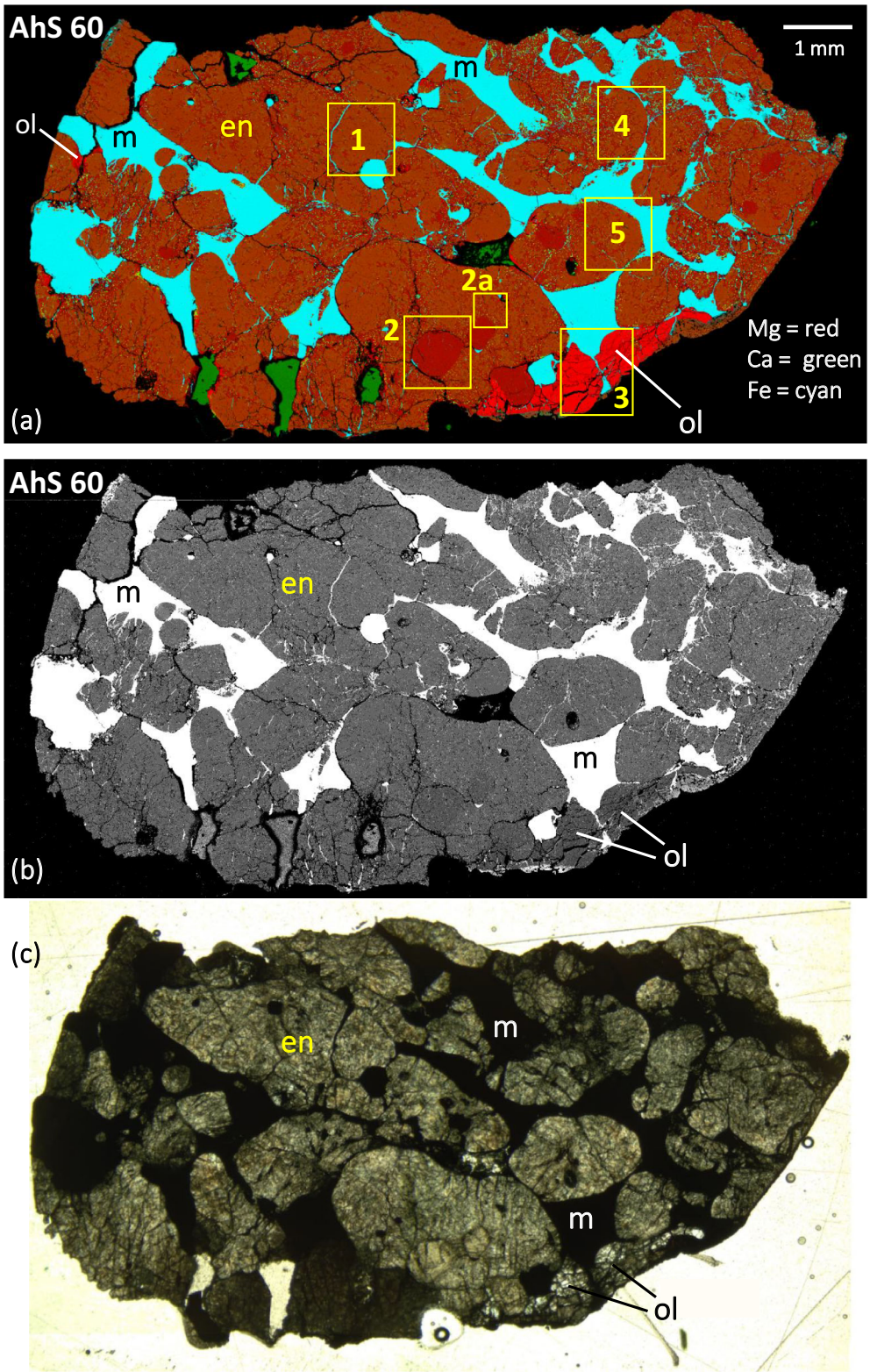

FIGURE 11. Studied section of AhS 60, an enstatite-rich achondrite. (a) Combined x-ray map (Mg = red; Ca = green; Fe = cyan). (b) BEI. (c) Transmitted light image. The main phases shown in the x-ray map are metal (cyan), olivine (bright red), and two intergmingled compositions of enstatite (Mg# 99.8 ± 0.1). The more abundant enstatite (brownish orange) has Wo ~3–4. The less abundant enstatite (darker red-orange) occurs mostly as irregular patches and veins in the former, and has Wo ~1. A few larger grains (e.g., area 2) are dominated by the low-Wo composition. ol = olivine; en = enstatite; m = metal. (Color figure can be viewed at wileyonlinelibrary.com)

19455100, 2024, 4, Downloaded from https://onlinelibrary.wiley.com/doi/10.1111/maps.14066 by University Of Wisconsin - Madison, Wiley Online Library on [18/06/2024]. See the Terms and Conditions (https://onlinelibrary.wiley.com/terms-and-conditions) on Wiley Online Library for rules of use; OA articles are governed by the applicable Creative Commons License

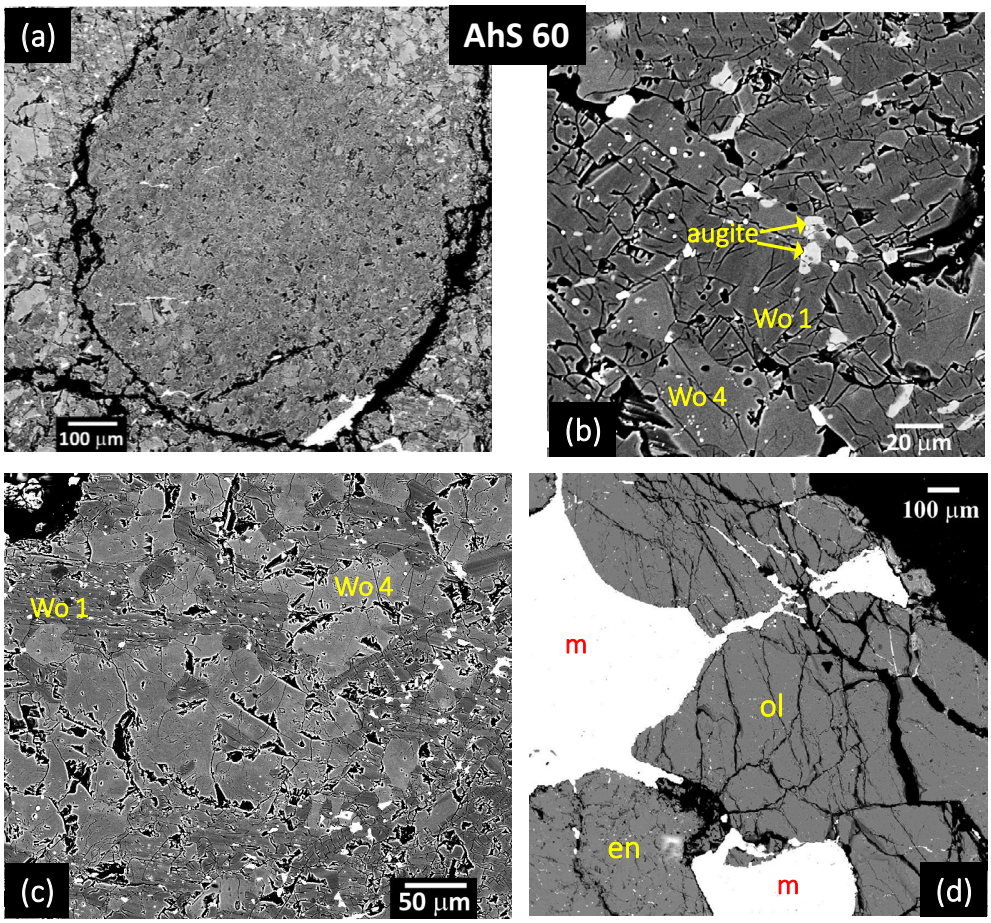

FIGURE 12. BEI of select areas of AhS 60. Note that (a, c, d) are rotated ~90° relative to the images in Figure 11. (a) Area 2 from Figure 11. This round area (once a single grain?) is dominated by the lower Wo enstatite (Wo ~1, darker in BEI), but is not completely homogeneous and shows intermingling of the two enstatite compositions around its borders. (b) Texture of the two enstatite compositions intermingled. The lower-Wo (darker) compositions contains small inclusions of augite. (c) Texture of the two enstatite compositions intermingled. Area 2a from Figure 11. (d) Olivine grains in area 3 from Figure 11. m = metal; en = enstatite; ol = olivine. (Color figure can be viewed at wileyonlinelibrary.com)

distribution of ureilitic types/compositions as that seen among main group ureilites (Downes et al., 2008; Goodrich et al., 2004; Goodrich, Hartmann, et al., 2015) strongly suggests that all ureilitic materials sampled on Earth, both main group and polymict ureilites, are derived from a single ureilitic daughter body.

Some authors have suggested that the non-ureilitic clasts in polymict ureilites were incorporated into ureilitic daughter bodies at the time of reassembly of these bodies, due to the presence of all kinds of chondritic debris in the region of nebula where the UPB disruption occurred (Bischoff et al., 2010; Herrin et al., 2010; Horstmann & Bischoff, 2014; Scott et al., 2018). However, Goodrich, Kring, et al. (2021) and Goodrich, Sanborn, et al. (2021) pointed out that the OC (as well as EC and RC) clasts in polymict ureilites include all petrologic types (3–6), which is critical because the higher petrologic types did not, in fact, exist (having been created by slow metamorphism at depth in their parent asteroids) until 30–50 Myr after CAI. This precludes the addition of most xenoliths at ~5 Ma after CAI. Based on this, Goodrich, Kring, et al. (2021) and Goodrich, Sanborn, et al. (2021) argued that most xenoliths were added to ureilitic regolith as remnants of impactors in a short period of time around 50 Myr after CAI, during a period of enhanced dynamical activity when many chondritic planetesimals of various types in the asteroid belt were disrupted and generated large amounts of excited materials.

The range of types of materials found as clasts in AhS is strikingly similar to that in TPUs. As shown by Goodrich, Bottke, et al. (2021), the range and relative abundances of ureilitic compositions and types is essentially identical. This is particularly significant because the observed distribution (which is also the same

19455100, 2024, 4, Downloaded from https://onlinelibrary.wiley.com/doi/10.1111/maps.14066 by University Of Wisconsin - Madison, Wiley Online Library on [18/06/2024]. See the Terms and Conditions (https://onlinelibrary.wiley.com/terms-and-conditions) on Wiley Online Library for rules of use; OA articles are governed by the applicable Creative Commons License

TABLE 6. Compositions of silicates in enstatite achondrite clast Almahata Sitta 60.

	Olivine		Pyroxene												
	Area 3		Area 1 light		Area 2 round dark grain		Area 2a dark		Area 2a light		Area 4 light		Area 5 dark	Area 5 light	
(#) analyses	(24)	SD	(23)	SD	(7)	SD	(6)	SD	(11)	SD	(16)	SD	(1)	(22)	SD
SiO_2	42.1	0.4	59.0	0.20	59.4	0.6	59.1	0.3	59.2	0.5	58.3	0.3	58.8	58.8	0.2
Al_2O_3	bdl		0.55	0.02	0.24	0.01	0.39	0.08	0.67	0.07	0.57	0.05	0.44	0.56	0.03
TiO_2	bdl		0.03	0.01	0.02	0.01	0.02	0.01	0.03	0.01	0.03	0.00	0.03	0.03	0.00
Cr_2O_3	bdl		bdl		bdl		bdl		bdl		bdl		bdl	bdl	
FeO	0.15	0.04	0.12	0.08	0.06	0.01	0.11	0.03	0.09	0.01	0.20	0.07	0.06	0.18	0.07
NiO	bdl		bdl		bdl		bdl		bdl		bdl		0.02	bdl	
MgO	56.9	0.2	38.1	0.18	39.2	0.4	38.6	0.4	37.9	0.3	38.0	0.2	38.9	38.2	0.2
MnO	0.05	0.01	0.05	0.01	0.04	0.01	0.06	0.02	0.06	0.01	0.06	0.01	0.03	0.06	0.01
CaO	0.15	0.01	1.58	0.08	0.48	0.02	0.72	0.06	2.07	0.24	1.65	0.18	0.66	1.63	0.11
Na_2O	bdl		0.02	0.01	bdl		bdl		bdl		0.02	0.01	bdl	0.02	0.01
Total	99.4	0.5	99.4	0.39	99.4	0.9	99.0	0.6	100.0	0.5	98.8	0.4	99.0	99.5	0.3
Fo/Mg#	99.9	0.0	99.8	0.1	99.9	0.0	99.8	0.0	99.9	0.0	99.7	0.1	99.9	99.7	0.1
En			96.9	0.1	99.0	0.0	98.5	0.0	96.1	0.0	96.7	0.1	98.7	96.8	0.1
Wo			2.9	0.1	0.9	0.0	1.3	0.1	3.8	0.4	3.0	0.3	1.2	3.0	0.2

Note: Areas are marked on Figure 8a. "light" and "dark" refer to appearance in backscattered electron images such as shown in Figure 12. Fo/Mg# = 100 × molar Mg/(Mg + Fe); En = 100 × molar Mg/(Mg + Fe + Ca); Wo = 100 × molar Ca/(Mg + Fe + Ca).
Abbreviations: bdl, below detection limit; SD = 1 sigma standard deviation.

among main group ureilites) is one that could not be due to igneous processes and is likely to be a result of selective sampling of the UPB during catastrophic disruption and reassembly (Goodrich, Hartmann, et al., 2015; Michel et al., 2015; Rai et al., 2020). Furthermore, both AhS and typical polymict ureilites contain clasts of feldspathic ureilitic lithologies (inferred to be UPB crustal materials) that do not occur among main group ureilites (Bischoff et al., 2014; Cohen et al., 2004; Goodrich, Collinet, Jercinovic, et al., 2022; Goodrich, Collinet, Treiman, et al., 2022 Goodrich, Treiman, et al., 2017), which further supports their essential similarity.

In terms of non-ureilitic materials, both AhS and TPUs contain clasts or fragments from every major class of chondrite (OC, EC, RC, and CC). In both cases, the OC clasts include all chemical groups (H, L, LL) and petrologic types. In both cases, the EC clasts or fragments include both chemical groups (EH and EL) and all petrologic types (Boleaga & Goodrich, 2019; Goodrich, Fioretti, et al., 2015; this work). Furthermore, in both cases, the dominant CC clasts are C1 lithologies of a distinct type that differs from any CC known as individual meteorites (Goodrich, Zolensky, Fioretti, et al. 2019; Goodrich, Zolensky, Kohl, et al., 2019). Nevertheless, there are also some apparent differences. Although RCs of a range of petrologic types occur in TPUs (Downes et al., 2008; Goodrich et al., 2016), the one "RC-like" clast reported in AhS appears to differ from known RC (Horstmann et al., 2010). The rare non-ureilitic achondrites that occur in TPUs (Goodrich, Mikouchi, et al., 2015; Goodrich, Kita, et al., 2017; Prinz et al., 1986) but have not been found in AhS. Also, the one CB found in AhS (Bischoff et al., 2012; Horstmann & Bischoff, 2014) is a meteorite type that has not been reported in TPUs. However, all these differences involve types of materials that are rare in either AhS or TPUs, and therefore, the statistics for comparison are poor. Considering that before this work, large clasts of EC had never been reported in TPUs, and that until recently CC had not been reported in AhS, it seems premature to base any arguments on the apparent absence of a particular type of clast. The majority of the >600 AhS stones in the UoK collection (Shaddad et al., 2010) have yet to be classified, and most of these are not from the large-mass area (Jenniskens et al., 2022) and so could include types of materials that differ from the strong EC and OC that preferentially survived as larger fragments. In addition, the majority of TPUs have not been scrutinized in any detail, while those that have been looked at have revealed a plethora of new types of materials in every polished section (e.g., Goodrich & Gross, 2015; Goodrich, Mikouchi, et al., 2015; Goodrich et al., 2016; Goodrich, Kita, et al., 2017; Goodrich, Ross, et al., 2017). Based on these considerations, we argue that apparent differences between the types of xenoliths found in AhS and those found in TPUs cannot necessarily be considered significant, and that such differences pale in comparison to the striking similarities.

19455100, 2024, 4, Downloaded from https://onlinelibrary.wiley.com/doi/10.1111/maps.14066 by University Of Wisconsin - Madison, Wiley Online Library on [18/06/2024]. See the Terms and Conditions (https://onlinelibrary.wiley.com/terms-and-conditions) on Wiley Online Library for rules of use; OA articles are governed by the applicable Creative Commons License

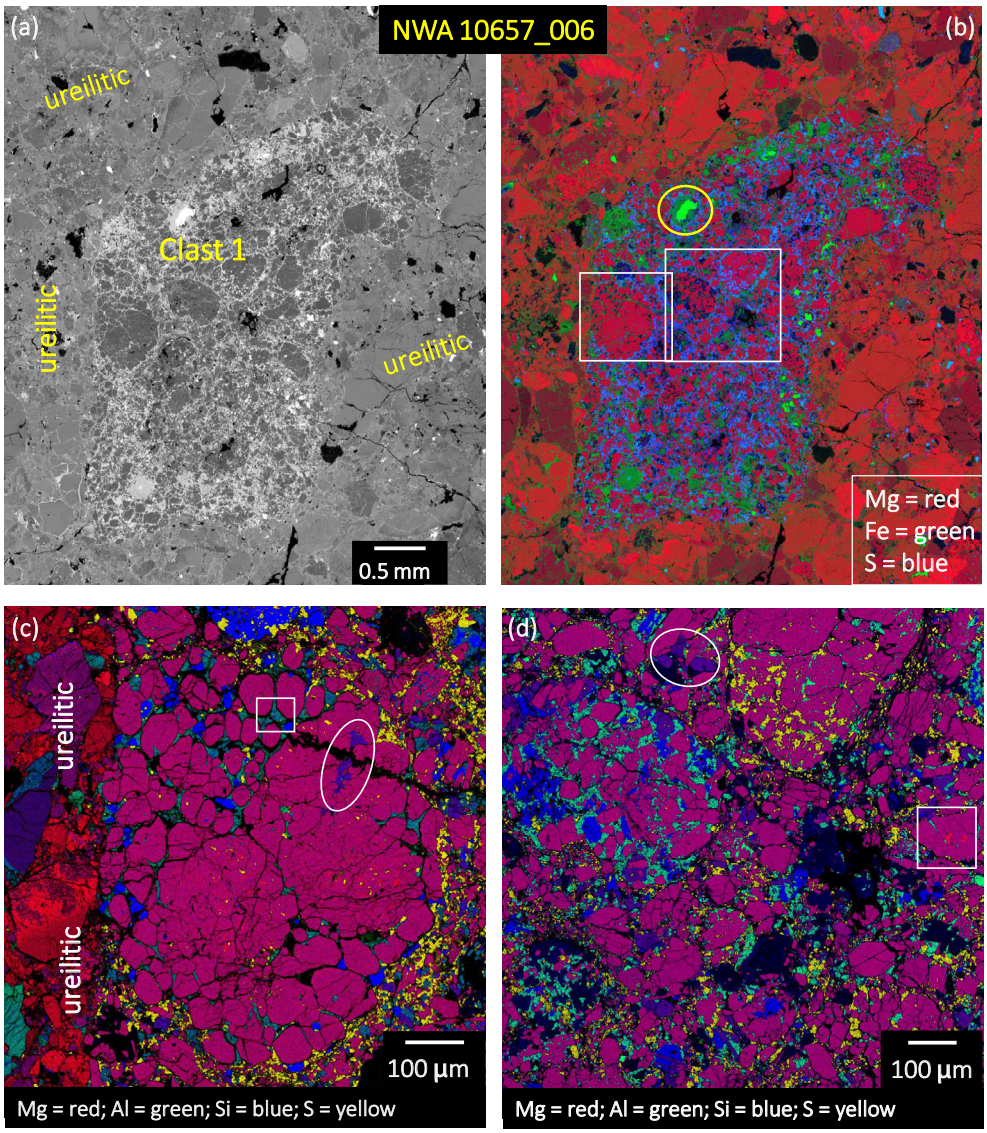

FIGURE 13. Clast 1, classified as an EH3, in polymict ureilite NWA 10657 (section_006). (a) BEI showing whole clast in matrix of ureilitic fragments. (b) Combined x-ray map (Mg = red; Fe = green; S = blue) showing whole clast in matrix of ureilitic fragments. (c) Combined x-ray map (Mg = red; Al = green; Si = blue; S = yellow) of area outlined by box on left in [b]. (d) Combined x-ray map (Mg = red; Al = green; Si = blue; S = yellow) of area outlined by box on right in [b]. (Color figure can be viewed at wileyonlinelibrary.com)

A model for formation of 2008 TC_3 (or its progenitor) and TPUs in the same regolith environment on a ureilitic daughter body was developed by Goodrich, Hartmann, et al. (2015); Goodrich, Zolensky, Fioretti, et al. (2019); Goodrich, Bottke, et al. (2021). We review the model briefly, and argue that our discovery of a large clast of an EC in a TPU strongly supports it. Typical polymict ureilites show clastic textures and a wide range of shock levels of clasts, and are well consolidated, that is, they are strong enough to survive atmospheric entry intact to become meteorites on Earth. They contain only sparse, heterogeneously distributed solar gases (Ott et al., 1993). These properties suggest that TPUs are derived from deep layers of mature regolith on a relatively large ureilitic daughter body (Figure 16a). In contrast, 2008 TC_3 was obviously weak and loosely consolidated; that is, it disintegrated in the atmosphere and only its strongest clasts survived to become the recovered stones. This may be because most of the asteroid was similar to the porous, fine-grained, highly shocked ureilitic AhS stones that provide a plausible match to its reflectance spectrum (Hiroi et al., 2010), suggesting that 2008 TC_3 was derived from shallow, poorly consolidated regions of the same regolith as TPUs (Figure 16a). Alternatively, the asteroid may have been dominated by C1 materials such as AhS 91A, which also matches the asteroid's spectrum

19455100, 2024, 4, Downloaded from https://onlinelibrary.wiley.com/doi/10.1111/maps.14066 by University Of Wisconsin - Madison, Wiley Online Library on [18/06/2024]. See the Terms and Conditions (https://onlinelibrary.wiley.com/terms-and-conditions) on Wiley Online Library for rules of use; OA articles are governed by the applicable Creative Commons License

TABLE 7. Compositions of silicates in clast 1 (enstatite chondrite) in NWA 10657_006.

	Olivine		Enstatite		"Melt"	Silica	
(#) analyses	(7)	SD	(41)	SD	(1)	(8)	SD
SiO_2	42.5	0.2	59.3	0.4	72.4	99.3	0.4
Al_2O_3	bdl		0.19	0.09	0.30	0.11	0.03
TiO_2	bdl		0.03	0.02	bdl	bdl	
Cr_2O_3	0.11	0.07	0.34	0.19	bdl	0.01	bdl
FeO	0.79	0.24	1.04	0.50	0.42	0.57	0.16
MgO	58.5	0.2	40.0	0.5	20.4	0.06	0.09
MnO	0.10	0.03	0.12	0.06	bdl	0.01	bdl
CaO	0.12	0.01	0.22	0.10	bdl	0.01	bdl
K_2O	bdl		bdl		2.9	0.01	0.01
Na_2O	bdl		bdl	0.01	4.2	0.02	0.01
Total	102.2	0.3	101.3	0.3	100.6	100.1	0.3
Fo/Mg#	99.3	0.2	98.6	0.7			
En			98.2	0.6			
Wo			0.4	0.2			

Note: Fo/Mg# = 100 × molar Mg/(Mg + Fe); En = 100 × molar Mg/(Mg + Fe + Ca); Wo = 100 × molar Ca/(Mg + Fe + Ca).
Abbreviations: bdl, below detection limit; SD, 1 sigma standard deviation.

and may be an even better match to its density and porosity and highly friable behavior (Goodrich, Zolensky, Fioretti, et al., 2019). In this case, 2008 TC_3 could have been derived from a volume of regolith dominated by a relatively large C1 impactor (Figure 16b). The presence of a large component of such material in the body on which 2008 TC_3 formed would, in fact, support the interpretation that this body is that same as that on which TPUs formed, since C1 xenoliths are the most abundant (volumetrically) type in TPUs.

Furthermore, formation of both AhS and TPUs in the same regolith pile could explain the apparent large difference in abundance of EC material between the two. The addition of impactor remnants to regolith is a stochastic process, resulting in local concentrations of xenolithic materials of different type that only become homogenized with other materials through extensive regolith processing. Thus, it is entirely plausible that 2008 TC_3 sampled a volume of regolith containing a concentration of EC materials (Figure 16a).

Bischoff et al. (2010, 2022) argued that the absence of solar gases in any AhS samples precludes formation of 2008 TC_3 in a regolith environment. However, this is not a strong argument because solar gases are only implanted in the top millimeter of an asteroidal surface (Wieler et al., 1986). Even extensive gardening may not redistribute such grains homogeneously in subsurface regolith layers and solar wind-bearing grains should generally be sparse in an extensive regolith (or mega-regolith) pile. Thus, the absence of solar gases in samples of either 2008 TC_3 or TPUs does not preclude formation in regolith.

The alternative model proposed by Bischoff et al. (2022) is that 2008 TC_3 was a polymict carbonaceous chondrite breccia that must have had an origin distinct from that of typical polymict ureilites. In this model, 2008 TC_3 formed as a late generation asteroid, 50–100 Myr after CAI, by re-accretion of C1 carbonaceous chondrite material (presumably following major disruption), along with fragments of ureilitic and other types of chondritic materials. We believe this model is implausible for several reasons. First, it is difficult to imagine how such a re-accreting body could have acquired such a strikingly similar mix of materials as that in TPUs. In particular, it is unlikely that it could have acquired the same range and distribution of ureilitic materials, because any other ureilitic daughter body (other than the one on which TPUs formed) that might have been available to provide such materials would have had a different mixture of materials from the original UPB (Michel et al., 2015). Moreover, reassembly following catastrophic disruption is not a viable mechanism for adding significant quantities of mixed foreign materials to a second-generation body, because the force driving the reassembly is the remembered gravitational attraction between the fragments ejected from the disrupted body (in this case, a CC), whereas other fragmental materials that might have been in the region would not share this attraction (Michel et al., 2001).

In summary, we argue that, by Occam's razor, the many similarities between the clast populations in AhS and TPUs strongly suggest a common origin in a regolith environment. Continued investigations of both TPUs and AhS may reveal additional discoveries, such as the CC recently found in AhS and the EC reported here in a TPU, which can be used to test this model.

Implications for the Histories of Enstatite Meteorite Asteroids

Comparison of AhS Enstatite Meteorite Clasts with Individual Enstatite Meteorites

Combining our results with the extensive previous work that has been done on AhS ECs, it can be seen that the range of types of EC material in AhS (in terms of chemical, petrologic, and oxygen isotopic properties) is not fundamentally different from what is seen in EC materials that have arrived at Earth in recent times as individual meteorites. The AhS EC have given us many fresh samples that provide new information, in particular on components such as metal and exotic sulfides that are highly susceptible to terrestrial weathering. This new information has been used to better address questions such as 1) whether type 3 EC are nebular condensates or impact melts (e.g., El Goresy et al., 2012; Horstmann et al., 2011),

19455100, 2024, 4, Downloaded from https://onlinelibrary.wiley.com/doi/10.1111/maps.14066 by University Of Wisconsin - Madison, Wiley Online Library on [18/06/2024]. See the Terms and Conditions (https://onlinelibrary.wiley.com/terms-and-conditions) on Wiley Online Library for rules of use; OA articles are governed by the applicable Creative Commons License

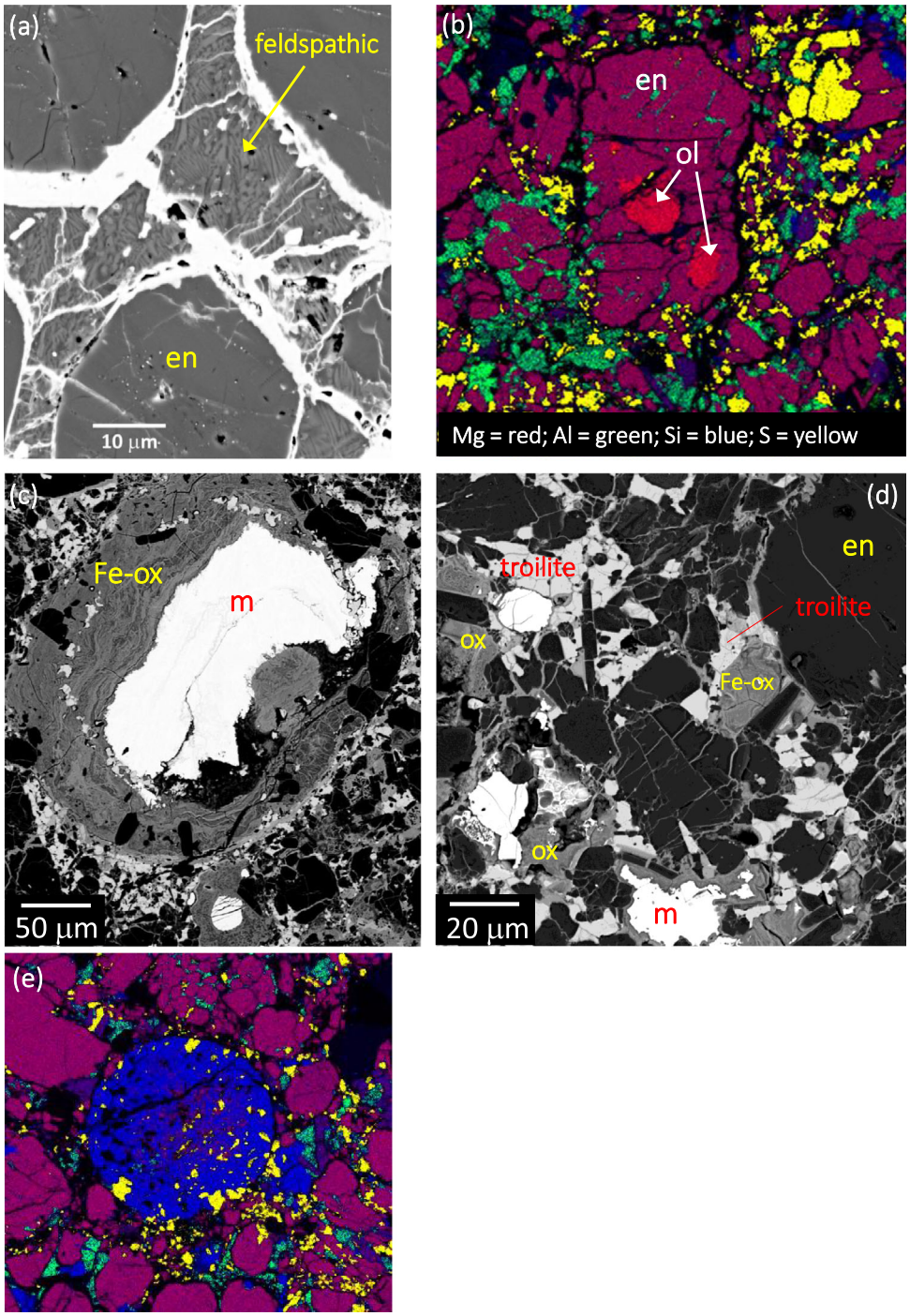

FIGURE 14. Images of clast 1 in NWA 10657_006. (a) BEI of feldspathic mesostasis in clast 1, area outlined by box in Figure 13c. (b) Combined x-ray map (Mg = red; Al = green; Si = blue; S = yellow) showing patches of olivine in enstatite grain in a chondrule in clast 1. (c) BEI of metallic spherule partially weathered (terrestrial alteration) to Fe-oxides (Fe-ox). (d) BEI showing terrestrial alteration to Fe-oxides (Fe-ox and ox) in clast 1. Patches of metal and troilite are preserved. (e) Chondrule consisting almost entirely of silica and minor sulfides (troilite) in clast 1. Combined x-ray map (Mg = red; Al = green; Si = blue; S = yellow). m = metal; en = enstatite; ol = olivine. (Color figure can be viewed at wileyonlinelibrary.com)

and 2) the origin of MSS (metal–silicate–sulfide intergrowths) in EC (Horstmann et al., 2014). In fact, Weyrauch et al. (2018) conducted a study of chemical variations of sulfides and metal in 45 EC, and almost half of these (22) were stones from AhS rather than individual meteorites. Studying this large data

19455100, 2024, 4, Downloaded from https://onlinelibrary.wiley.com/doi/10.1111/maps.14066 by University Of Wisconsin - Madison, Wiley Online Library on [18/06/2024]. See the Terms and Conditions (https://onlinelibrary.wiley.com/terms-and-conditions) on Wiley Online Library for rules of use; OA articles are governed by the applicable Creative Commons License

TABLE 8. Compositions of metal, phosphide, and sulfide in clast 1 (enstatite chondrite) in NWA 10657_006.

	Metal				
	avg (52)	SD	Phosphide	Troilite	Troilite
P	0.18	0.11	14.92	0.01	0.01
S	bdl		0.10	39.0	36.9
Si	2.8	0.21	0.24	0.04	0.03
Mg	bdl		bdl	0.02	0.02
Fe	87.5	1.8	77.2	57.1	60.0
Ni	8.8	1.9	7.84	0.70	0.09
Co	0.32	0.02	0.25	bdl	bdl
Cr	bdl		0.01	1.8	1.8
Mn	bdl		bdl	0.12	0.14
Ti	0.01	0.01	0.01	0.27	0.29
Total	99.6		100.5	99.0	99.3

Abbreviations: bdl, below detection limit; SD = 1 sigma standard deviation.

set allowed Weyrauch et al. (2018) to recognize that there are four major subgroups of EC (EH_a, EL_a, EH_b, EL_b, which we have used here), which has helped to clarify some of previously observed variations, for example, in compositions of Fe-Mn-Mg sulfides (alabandite versus keilite) in EL. It is notable that the AhS samples used in that study do not stand out as a unit, but are spread among all four subgroups. Thus, the AhS EC have added to our knowledge of EC by adding many fresh samples to our collections and improving statistics, but have not revealed any new EC types. The only type of enstatite achondrite found so far in AhS (samples AhS 60, MS-MU-019, and MS-MU-036), does constitute a type that has never been found as an individual meteorite.

Number and Sizes of Enstatite Meteorite Parent Asteroids

The number of parent bodies giving rise to EC meteorites is uncertain. Keil (1984) argued that there must at least have been different parent bodies for EH and EL. In contrast, Kong et al. (1997) argued that there is continuity in bulk rock compositional data between EH and EL, and therefore, they may have come from a single parent body. However, based on the larger data set of EC afforded by AhS, Weyrauch et al. (2018) identified compositionally distinct groups (two EH and two EL) requiring at least four parent bodies. The existence of several anomalous ECs could increase that number to greater than 10 (Goss et al., 2023; Grossman et al., 1993; Lin & Kimura, 1998; Rindlisbacher et al., 2021; Weisberg & Kimura, 2012; Weyrauch et al., 2018; Zhang et al., 1995). Furthermore, Keil and Bischoff (2008) concluded that the known enstatite achondrites could represent another three original EC bodies (aubrites, Shallowater, NWA 2526/Itqiy), while Barrat et al. (2016) concluded that the aubrites themselves required two bodies. The unique enstatite achondrite lithology in AhS, represented by AhS 60 in this work and MS-MU-019 and MS-MU-036 (Harries & Bischoff, 2020), clearly appears to be genetically related to EC, based on its oxygen isotope composition (Figure 15a), and so adds yet another EC parent body to the count.

Previous oxygen isotope data for ECs have not shown any subgroups that clearly correlate with chemical or petrologic properties and might be used to distinguish different parent bodies. Instead, the range of $\Delta^{17}O$ shown by EC falls is likely a feature of primitive EC materials and may be a result of heterogeneous distribution of primordial components with a broad range of $\Delta^{17}O$ values (Weisberg et al., 2021; Zhu et al., 2020). The oxygen isotope data for the AhS EC confirm this observation. Combining all data from this work and Horstmann and Bischoff (2014) for AhS EC (Figure 15b), we find that there is no correlation between oxygen isotope composition and chemical group (EH or EL) or subgroup ("a" or "b").

The sizes of the EC parent bodies are also unknown. Based on a thermal model for EL6s, Trieloff et al. (2022) estimated a parent body diameter of 120–160 km, which they argue is comparable to the H or L parent body. In fact, EC parent body sizes are likely to have been similar to those of OC because equilibration temperatures for type 4–6 EC are similar to those of equivalent petrologic type OC (Dodd, 1981; Huss et al., 2006; Zhang et al., 1995), although previous estimates for OC span a large range from ~160 to 300 km diameter (Bennett & McSween Jr, 1996; Blackburn et al., 2017; Miyamoto et al., 1981; Pellas & Fieni, 1988).

Keil et al. (1989) inferred a diameter of 100 km for the parent body of the Shallowater enstatite achondrite. Harries and Bischoff (2020) inferred a much larger body, on the order of 500 km, for the AhS EC lithology (AhS 60, MS-MU-019, and MS-MU-036). They identified the coexisting high-Wo and low-Wo phases in this lithology as low-temperature orthoenstatite and low-temperature clinoenstatite, respectively, and argued from phase relations that formation of this assemblage required a pressure of ~0.1 GPa. However, they also discussed the possibility of metastable formation at low pressure, which would be consistent with the suggestion of Goodrich et al. (2018) that AhS 60 was an annealed impact melt rock.

Breakup of Enstatite Meteorite Asteroids

The observation that the EC clasts in polymict ureilites are not fundamentally different from individual

19455100, 2024, 4, Downloaded from https://onlinelibrary.wiley.com/doi/10.1111/maps.14066 by University Of Wisconsin - Madison, Wiley Online Library on [18/06/2024]. See the Terms and Conditions (https://onlinelibrary.wiley.com/terms-and-conditions) on Wiley Online Library for rules of use; OA articles are governed by the applicable Creative Commons License

TABLE 9. Oxygen isotope compositions of EC clasts from Almahata Sitta (AhS).

Sample	$\delta^{17}O‰$	1σ	$\delta^{18}O‰$	1σ	$\Delta^{17}O‰$	1σ	$\Delta^{17}O‰_{linear}$	1σ
AhS 1002	3.206		6.071		0.049		0.025	
AhS 1002	3.200		6.043		0.058		0.034	
Mean values	3.203	0.004	6.057	0.020	0.053	0.006	0.029	0.006
AhS 26	3.138		6.014		0.011		−0.013	
AhS 26	3.101		5.935		0.015		−0.009	
Mean values	3.120	0.026	5.975	0.056	0.013	0.003	−0.011	0.003
AhS S151	2.619		5.552		−0.268		−0.290	
AhS S151	2.579		5.496		−0.279		−0.300	
Mean values	2.599	0.028	5.524	0.040	−0.273	0.008	−0.295	0.008
AhS 2012	3.155		6.031		0.019		−0.005	
AhS 2012	3.363		6.430		0.019		−0.006	
Mean values	3.259	0.147	6.231	0.282	0.019	0.000	−0.005	0.001
AhS 41	2.971		5.663		0.026		0.004	

Note: $\Delta^{17}O$ ‰linear calculated as in Miller (2002).

EC meteorites implies that fragments of the same populations of EC parent bodies were available as impactors at two very different times, that is, at ~50–60 Myr after CAI and recently. A similar observation was made about the OC clasts in AhS and TPUs (Goodrich, Kring, et al., 2021). The fact that the EC clasts (like the OC) include the entire known range of EC chemical groups and petrologic types implies that the materials that were available to be implanted into ureilitic daughter bodies at ~50–60 Myr after CAI must have been derived from a large range of depths in several (at least five) EC parent bodies, that is, consistent with the interpretation that this was a period of enhanced dynamical activity when many chondritic planetesimals of various types in the asteroid belt were disrupted (Goodrich, Kring, et al., 2021; Goodrich, Sanborn, et al., 2021). A $^{40}Ar/^{39}Ar$ age of 4513 ± 16 Ga for an EL6 AhS clast (MS-D), interpreted as recording the time of cooling to the Ar closure temperature on the parent asteroid, is also consistent with this interpretation (Turrin et al., 2023).

The excavated EC materials could have directly become impactors onto ureilitic bodies. Alternatively, they may have reassembled as mixed layers containing materials from a large range of depths, on the surfaces of each of the original EC bodies, and been subsequently ejected by subcatastrophic impacts. The existence of the EL breccia MS-179, containing clasts of a range of petrologic types, attests to such mixing prior to impact ejection and implantation into AhS (Bischoff et al., 2022). As argued for the OC (Goodrich, Kring, et al., 2021), formation of mixed outer layers of reaccreted materials (rubbly layers), rather than complete parent body disruption, is more likely because it could leave relatively large EC bodies (e.g., >100 km diameter, as inferred from thermal modeling) intact. This means that they could still be available to be catastrophically disrupted more recently and deliver EC to Earth as individual meteorites, whereas complete disruption of the original parent bodies at 50 Myr after CAI would have left much smaller EC fragments or daughter bodies that would have been unlikely to survive for 4 billion years. It is also consistent with the extensive evidence of shock metamorphism and melting in EC, which suggests multiple impact events (Fagan et al., 2000; McCoy et al., 1995; Rubin, 1997; Rubin, 2015; Rubin & Scott, 1997a, 1997b; Udry et al., 2019; Van Niekerk & Keil, 2011).

These arguments likely apply to the EC-like parent asteroids of enstatite achondrites (or at least some of them) as well, although this is less certain because no specific genetic relationships between enstatite achondrites and EC have ever been established. In addition, the significance of the unique AhS 60-like enstatite achondrite in AhS is uncertain. This lithology may have been derived from an EC-like body that was largely destroyed around 50 Myr after CAI and did not survive to deliver individual meteorites to Earth in recent times.

Implications for Dynamical Evolution of the Solar System

The EC and other non-ureilitic clasts in polymict ureilites provide a snapshot of what may have been a critical timestep in the collisional and dynamical evolution of the early solar system. The locations at which solar system bodies accreted have been inferred from various nucleosynthetic isotope systems (Kleine et al., 2020; Warren, 2011). Yamakawa et al. (2010) noted a linear correlation of $\varepsilon^{54}Cr$ with heliocentric distance for Earth, Mars, and Vesta (HED meteorites), which could be extrapolated to place the UPB at ~2.8 AU. If EC and OC can be included in this trend, their locations would be at ~1 and ~2 AU, respectively. In other words, EC, OC, and ureilitic asteroids were well separated from one

19455100, 2024, 4, Downloaded from https://onlinelibrary.wiley.com/doi/10.1111/maps.14066 by University Of Wisconsin - Madison, Wiley Online Library on [18/06/2024]. See the Terms and Conditions (https://onlinelibrary.wiley.com/terms-and-conditions) on Wiley Online Library for rules of use; OA articles are governed by the applicable Creative Commons License

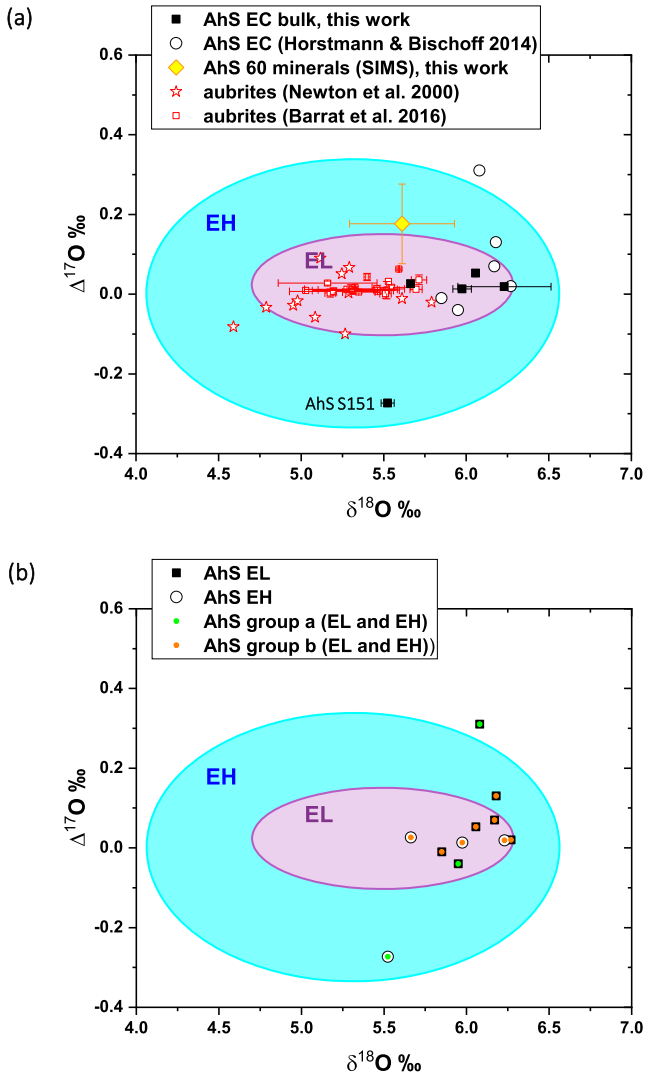

FIGURE 15. (a) Oxygen isotope compositions of the AhS EC clasts studied in this work, compared with AhS EC from Horstmann and Bischoff (2014). Also shown is the mean composition of olivine and pyroxene in AhS 60 enstatite achondrite from SIMS analyses in this work, compared with compositions of aubrites from Newton et al. (2000) and Barrat et al. (2016). (b) Oxygen isotope compositions of all AhS EC clasts from this work and Horstmann and Bischoff (2014). Data are plotted to distinguish EH and EL, and group "a" and group "b". There are no obvious correlations of oxygen isotope composition with chemical group or subgroup. Fields for EH and EL chondrites are from Greenwood et al. (2017) and show 2 sigma variation of the means for each group based on data of Newton et al. (2000). (Color figure can be viewed at wileyonlinelibrary.com)

another originally in the inner solar system. And yet, at 50–60 Myr after CAI, they were in close enough proximity in the asteroid belt that abundant fragments of them could become collisionally mixed with one another. This implies significant migration of these asteroids from their formation locations, which is consistent with the currently observed compositional diversity of the asteroid belt (DeMeO & Carry, 2014). Goodrich, Kring, et al. (2021) and Goodrich, Sanborn, et al. (2021) argued that the CC clasts in polymict ureilites were derived from originally outer solar system bodies that had migrated into the inner solar system at 3–5 Ma after CAI, as described in dynamical models such as the Grand Tack (Walsh et al., 2012), and thus were available to be disrupted there at ~50 Myr after CAI along with multiple EC and OC bodies. A Grand Tack type event would have also resulted in substantial excitation and mixing of inner solar system bodies (Walsh et al., 2012), which might provide the migrations necessary to put OC, EC, and ureilitic bodies close together. The Grand Tack model is currently only one of several competing dynamical models for early planetary and planetesimal migrations (e.g., Clement et al., 2018, 2019; de Sousa et al., 2020). Evaluating such models is beyond the scope of this work, but we suggest that polymict ureilites can be used as a crucial constraint in doing so.

Of course, in more recent times, EC, OC, and ureilitic asteroids must have been transferred to Earth-crossing orbits via dynamical resonances and the Yarkovsky effect. We do not know which asteroid or asteroid family gave rise to 2008 TC_3 (and/or other ureilites), although Jenniskens et al. (2010) and Gayon-Markt et al. (2012) identified some low-inclination near-Earth asteroids with spectra similar to 2008 TC_3 and considered several Main belt asteroid families as possible source regions for this population. Similarly, we do not know whence present-day EC falls originate, although the Hungaria asteroid family has been suggested as a possible source of the aubrite enstatite achondrites (Ćuk et al., 2014). What polymict ureilites (both AhS and other polymict ureilites) suggest is that both EC and ureilites may have come via similar routes.

SUMMARY AND CONCLUSIONS

- We studied the petrology of seven ECs and one enstatite achondrite from the UoK collection of AhS samples. Most of the studied samples were recovered from the far end of the 2008 TC_3 strewn field in which the largest masses fell. We obtained oxygen isotope compositions for five of the chondrites and for the achondrite.
- We discovered the first bona fide (3.5 mm-sized) clast of an EC in a typical polymict ureilite (NWA 10657) and studied its petrology.
- Using mineralogical, mineral compositional, and textural criteria, we find that the seven AhS EC studied comprise one EH_a3 (S151), one EL_b3 (AhS 1002), two EH_b4-5 (AhS 2012, AhS 26), two EH_b5-6 or possibly impact melt rocks (AhS 609, AhS 41), and

19455100, 2024, 4, Downloaded from https://onlinelibrary.wiley.com/doi/10.1111/maps.14066 by University Of Wisconsin - Madison, Wiley Online Library on [18/06/2024]. See the Terms and Conditions (https://onlinelibrary.wiley.com/terms-and-conditions) on Wiley Online Library for rules of use; OA articles are governed by the applicable Creative Commons License

TABLE 10. Oxygen isotope compositions of AhS 60 enstatite achondrite from SIMS.

Area	Data #	Phase	Fo or En[a]	Wo[a]	$\delta^{18}O‰$	Unc.[b]	2SD[c]	$\delta^{17}O‰$	Unc.[b]	2SD[c]	$\Delta^{17}O$	Unc.[b]	2SD[c]
AhS60-Area 3_8	324	ol	99.8		5.42	0.26		3.20	0.23		0.38	0.24	
AhS60-Area 3_6_7	325	ol	99.9		5.42	0.26		3.13	0.23		0.31	0.24	
AhS60-Area 3_11	330	ol	99.9		5.48	0.26		3.00	0.23		0.15	0.24	
AhS60-Area 3_20	331	ol	99.9		5.48	0.26		3.00	0.23		0.15	0.24	
AhS60-Area 1_1	320	px	97.1	2.8	5.70	0.26		3.10	0.23		0.14	0.24	
AhS60-Area 1_13	321	px	97.1	2.8	5.55	0.26		3.19	0.23		0.30	0.24	
AhS60-Area 2_24	322	px	98.9	1.0	5.85	0.26		3.17	0.23		0.12	0.24	
AhS60-Area 2_51	323	px	95.8	4.1	5.47	0.26		2.92	0.23		0.07	0.24	
AhS60-Area 4_2	332	px	97.0	2.9	5.67	0.26		3.02	0.23		0.08	0.24	
AhS60-Area 4_7	333	px	97.0	2.9	5.70	0.26		3.08	0.23		0.12	0.24	
AhS60-Area 5_20	334	px	97.0	2.8	5.75	0.26		3.31	0.23		0.32	0.24	
AhS60-Area 5_29	335	px	97.0	2.8	5.84	0.26		3.01	0.23		−0.03	0.24	
AhS 60, Mean (n = 12)					5.61	0.32	0.32	3.09	0.18	0.22	0.18	0.10	0.25

[a]Fo (for olivine) = 100 × molar Mg/(Mg + Fe). En (for pyroxene) = 100 × molar Mg/(Mg + Fe + Ca); Wo (for pyroxene) = 100 × molar Ca/(Mg + Fe + Ca).
[b]Uncertainties of individual analyses correspond to the external uncertainties of San Carlos olivine running standard (2SD, n = 12). Uncertainties of the mean include propagated uncertainties of individual analyses, instrumental bias correction (0.3‰ and 0.15‰ for $\delta^{18}O$ and $\delta^{17}O$, respectively), uncertainties of the mean of standard analyses (0.07‰ for $\delta^{18}O$, $\delta^{17}O$, and $\Delta^{17}O$), and small variations in measured $\delta^{18}O$ for olivine and pyroxene analyses (0.32‰).
[c]Twice the standard deviation (2SD) of 12 unknown analyses.

Table 11. Classification parameters for EC clasts in this study. (Color table can be viewed at wileyonlinelibrary.com)

	EH						EL	
	AhS S151	AhS 2012	AhS 609	AhS 41	AhS 26	Clast 1[a]	AhS 17	AhS 1002
Si in metal (wt%)	3.1	2.5	2.4	2.5	2.5	2.8	1.1	1.5
Cr in troilite (wt%)	1.1	2.9	2.6	2.7	2.6	1.8	3.1	2.8
Fe in Fe-Mn-Mg sulfide (wt%)	18.1	26.6	36.1	35.8	26.1	nd	38.1	38.2
Presence of daubreelite	Yes	Yes	nd	nd	nd	nd	nd	nd
Presence of olivine	Yes					Yes		Yes
Petrologic type based on textures	3	4–5	5–6	6	4–5	3	6–7	3
Classification	EH_a3	EH_b4-5	EH_b5-6	EH_b5-6	EH_b4-5	EH_b3	EL_b6-7	EL_b3

Note: Color coding: gold = group a, green = group b (Weyrauch et al., 2018).
Abbreviation: nd, not determined.
[a]In NWA 10657_006.

one EL_b6-7 (AhS 17), and the EC clast in NWA 10657 is EH_a3. Oxygen isotope compositions of all clasts analyzed are similar to those of EC from non-UoK collections of AhS, and within the range of compositions of individual EC meteorites. There are no correlations of oxygen isotope composition with chemical group or subgroup.

- The EC clasts from the UoK collection show the same large range of types as those from non-UoK collections of AhS. The enstatite achondrite, AhS 60, is a unique type (i.e., not known as an individual meteorite) that is also found among non-UoK AhS samples.
- The discovery of a large clast of an EC in a typical polymict ureilite eliminates what was thought to be a major difference in types of non-ureilitic materials found in AhS versus typical polymict ureilites.
- We argue that the range of types of both ureilitic and non-ureilitic materials in AhS and typical polymict ureilites are essentially similar, strongly indicating a common origin. We elaborate upon a previously proposed model in which AhS and typical polymict ureilites formed in the same regolith environment on a ureilitic daughter body. Most non-ureilitic clasts are remnants of impactors implanted into this regolith at ~50–60 Myr after CAI. Differences in relative abundances of types are due to the stochastic nature of impactor additions to regolith.
- There is no significant difference between the range of types of EC in polymict ureilites compared with

19455100, 2024, 4, Downloaded from https://onlinelibrary.wiley.com/doi/10.1111/maps.14066 by University Of Wisconsin - Madison, Wiley Online Library on [18/06/2024]. See the Terms and Conditions (https://onlinelibrary.wiley.com/terms-and-conditions) on Wiley Online Library for rules of use; OA articles are governed by the applicable Creative Commons License

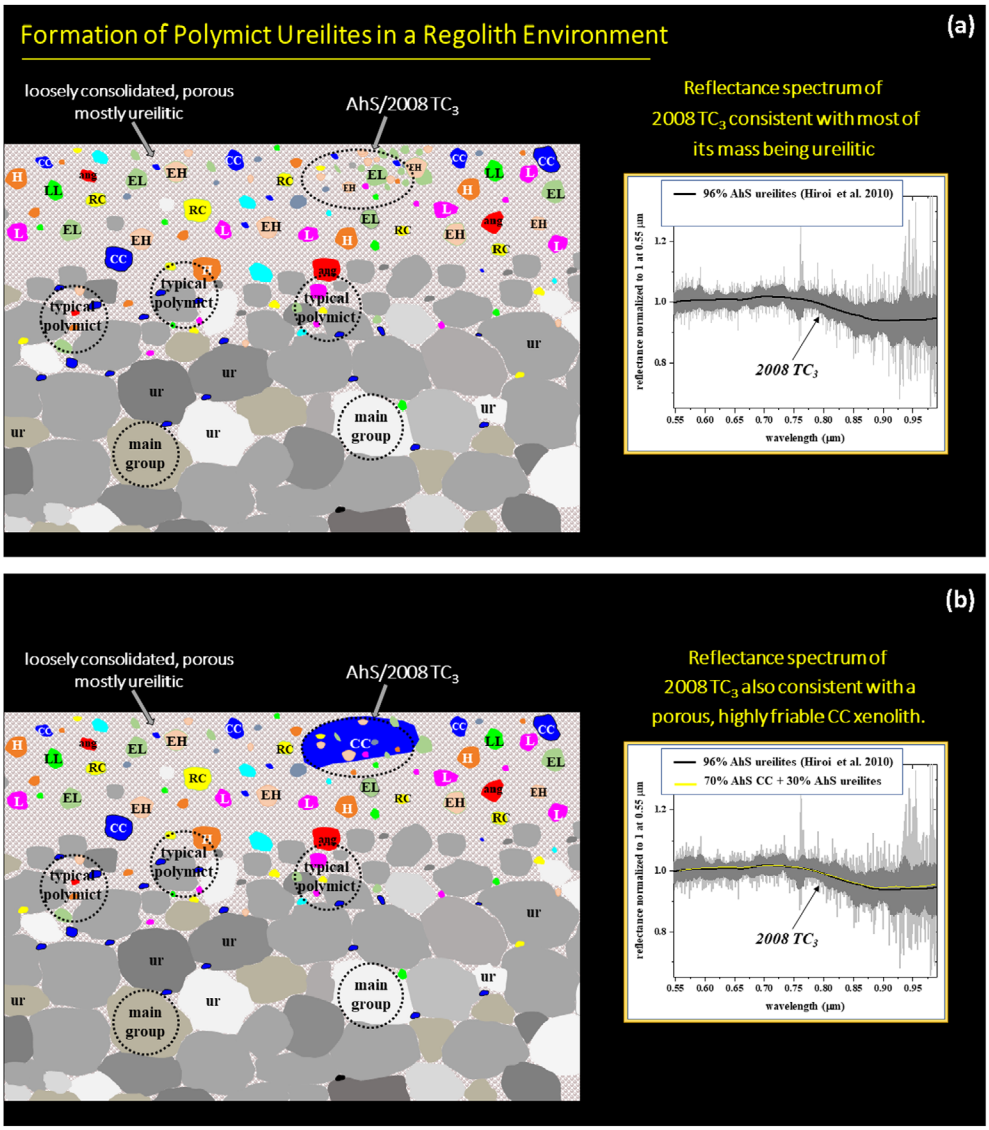

FIGURE 16. Proposed model for formation of asteroid 2008 TC_3 (i.e., its progenitor asteroid) in the same regolith environment as typical polymict ureilites. (a) Illustrates the case in which 2008 TC_3 consisted dominantly of ureilitic materials, while (b) illustrates the case in which 2008 TC_3 consisted mostly of C1 carbonaceous chondrite material. Based on the reflectance spectrum of the asteroid, these two possibilities cannot be distinguished. (a) Shows that 2008 TC_3 could have sampled a volume with a relatively high abundance of EC material, due to the stochastic nature of impactor addition, and subsequent long-lasting heterogeneity, of regolith. (Color figure can be viewed at wileyonlinelibrary.com)

individual EC meteorites. This implies that fragments of the same populations of EC parent bodies were available as impactors at two very different times, that is, at ~50–60 Myr after CAI, and recently. This can be explained if the materials that were excavated from EC parent bodies by major impacts at ~50–60 Myr after CAI were reassembled into mixed rubbly layers on the surfaces of each of those bodies, leaving relatively large EC bodies intact so they could survive 4 billion years to provide meteorites to Earth.

- The EC and other non-ureilitic clasts in polymict ureilites record a critical timestep in the collisional and dynamical evolution of the solar system. Although EC, OC, and ureilitic asteroids probably accreted at significantly different locations (1, 2, and 2.8 AU, respectively), at 50–60 Myr after CAI they were in close enough proximity to one another in the asteroid belt that abundant fragments of them (plus other types) could become collisionally mixed. This implies significant early planetesimal migrations.

19455100, 2024, 4, Downloaded from https://onlinelibrary.wiley.com/doi/10.1111/maps.14066 by University Of Wisconsin - Madison, Wiley Online Library on [18/06/2024]. See the Terms and Conditions (https://onlinelibrary.wiley.com/terms-and-conditions) on Wiley Online Library for rules of use; OA articles are governed by the applicable Creative Commons License

Polymict ureilites provide crucial constraints on the dynamical processes that resulted in these migrations.

Acknowledgments—We are indebted to Edward R. D. Scott for his extensive work on ECs, ureilites, and AhS, only a fraction of which we have been able to cite in this paper. We thank UoK staff and students for supporting the AhS meteorite recovery and sample handling. We thank Mike Zolensky for the loan of section AhS 41. We thank Kent Ross (JSC), Loan Le (JSC), Aaron Bell (UC, Boulder), and John Spratt (NHM) for assistance with electron microprobe analyses and/or x-ray mapping, David Mittlefehldt and Jason Herrin for help with the LA-ICPMS analyses, and Kohei Fukuda and Michaelle Spicuzza (U Wisconsin-Madison) for assistance with SIMS instrument. We thank William Bottke for interesting and helpful discussions. We greatly appreciate helpful reviews from Michael Weisberg, Alan Rubin, and the Associate Editor Sasha Krot, which led to improvements in this manuscript. This work was supported by NASA grant 80NSSC19K0507 (Emerging Worlds). WiscSIMS is partly supported by NSF (EAR2004618). This is LPI contribution #2998.

Data Availability Statement—All supporting data will be published as supplementary material.

Editorial Handling—Dr. Alexander Krot

REFERENCES

Barrat, J. A., Greenwood, R. C., Keil, K., Rouget, M. L., Boesenberg, J. S., Zanda, B., and Franchi, I. A. 2016. The Origin of Aubrites: Evidence from Lithophile Trace Element Abundances and Oxygen Isotope Compositions. *Geochimica et Cosmochimica Acta* 191: 29–48.

Bendersky, C., Weisberg, M. K., Connolly, H. C., Jr., and Ebel, D. S. 2007. Olivine and the Onset of Thermal Metamorphism in EH3 Chondrites. 38th Lunar and Planetary Science Conference, abstract #2077.

Bennett, M. E., and McSween, H. Y., Jr. 1996. Revised Model Calculations for the Thermal Histories of Ordinary Chondrite Parent Bodies. *Meteoritics & Planetary Science* 31: 783–792.

Bischoff, A., Bannemann, L., Decker, S., Ebert, S., Haberer, S., Heitmann, U., Horstmann, M., et al. 2022. Asteroid 2008 TC_3, Not a Polymict Ureilitic but a Polymict C1 Chondrite Parent Body? Survey of 249 Almahata Sitta Fragments. *Meteoritics & Planetary Science* 57: 1339–64.

Bischoff, A., Ebert, S., Patzek, M., Horstmann, M., Pack, A., Barratt, J.-A., and Decker, S. 2015. New Individuals from the Almahata Sitta Strewn Field: Old Friends and Brand-New Fellows. 78th Meeting of Meteoritical Society, Abstract #5092.

Bischoff, A., Ebert, S., Patzek, M., Horstmann, M., Pack, A., and Decker, S. 2016. Almahata Sitta News: Well-Known Varieties and New Species in the Zoo. 79th Annual Meeting of the Meteoritical Society, abstract #6319.

Bischoff, A., Horstmann, M., Barrat, J.-A., Chaussidon, M., Pack, A., Herwartz, D., Ward, D., Vollmer, C., and Decker, S. 2014. Trachyandesitic Volcanism in the Early Solar System. *Proceedings of the National Academy of Sciences of the United States of America* 111: 12689–92.

Bischoff, A., Horstmann, M., Heusser, G., Pack, A., and Albrecht, M. 2012. Almahata Sitta Sample MS-181: The First Carbonaceous Chondrite (CBa) from Asteroid 2008 TC_3. 75th Annual Meeting of the Meteoritical Society, abstract #5053.

Bischoff, A., Horstmann, M., Pack, A., Laubenstein, M., and Haberer, S. 2010. Asteroid 2008 TC_3-Almahata Sitta: A Spectacular Breccia Containing Many Different Ureilitic and Chondritic Lithologies. *Meteoritics & Planetary Science* 45: 1638–56.

Bischoff, A., Scott, E. R. D., Metzler, K., and Goodrich, C. A. 2006. Nature and Origins of Meteoritic Breccias. In *Meteorites and the Early Solar System II*, edited by D. S. Lauretta, and H. Y. McSween, Jr., 679–714. Tucson, AZ: University of Arizona Press.

Blackburn, T., Alexander, C. M. O.'. D., Carlson, R., and Elkins-Tanton, L. T. 2017. The Accretion and Impact History of the Ordinary Chondrite Parent Bodies. *Geochimica et Cosmochimica Acta* 200: 201–217.

Boleaga, Y., and Goodrich, C. A. 2019. Xenolithic Fe,Ni Metal in Polymict Ureilite Meteorites. 50th Lunar and Planetary Science Conference, abstract #1662.

Borovička, J., and Charvát, Z. 2009. Meteosat Observation of the Atmospheric Entry of 2008 TC_3 over Sudan and the Associated Dust Cloud. *Astronomy and Astrophysics* 507: 1015–22.

Boyet, M., Bouvier, A., Frossard, P., Hammouda, T., Garcon, M., and Gannoun, A. 2018. Enstatite Chondrites EL3 as Building Blocks for the Earth: The Debate over the ^{146}Sm-^{142}Nd Systematics. *Earth and Planetary Science Letters* 488: 68–78.

Brearley, A. J., and Jones, R. H. 1998. Chondritic Meteorites. In *Planetary Materials*, edited by J. J. Papike. Reviews in Mineralogy, vol. 36. Washington, DC: Mineralogical Society of America, pp. 3-01–3-170.

Campbell, A. J., and Humayun, M. 1999. Microanalysis of Platinum Group Elements in Iron Meteorites Using Laser Ablation ICP-MS. 30th Lunar and Planetary Science Conference, abstract #1974.

Campbell, A. J., and Humayun, M. 2005. Compositions of Group IVB Iron Meteorites and their Parent Melt. *Geochimica et Cosmochimica Acta* 69: 4733–44.

Campbell, A. J., Humayun, M., and Weisberg, M. K. 2002. Siderophile Element Constraints on the Formation of Metal in the Metal-Rich Chondrites Bencubbin, Weatherford, and Gujba. *Geochimica et Cosmochimica Acta* 66: 647–660.

Clement, M. S., Kaib, N. A., Raymond, S. N., and Walsh, K. J. 2018. Mars' Growth Stunted by an Early Giant Planet Instability. *Icarus* 311: 340–356.

Clement, M. S., Kaib, N. A., Raymond, S. N., and Walsh, K. J. 2019. The Early Instability Scenario: Terrestrial Planet Formation during the Giant Planet Instability, and the Effect on Collisional Fragmentation. *Icarus* 321: 778–790.

Cohen, B. A., Goodrich, C. A., and Keil, K. 2004. Feldspathic Clast Populations in Polymict Ureilites: Stalking the Missing Basalts from the Ureilite Parent Body. *Geochimica et Cosmochimica Acta* 68: 4249–66.

19455100, 2024, 4, Downloaded from https://onlinelibrary.wiley.com/doi/10.1111/maps.14066 by University Of Wisconsin - Madison, Wiley Online Library on [18/06/2024]. See the Terms and Conditions (https://onlinelibrary.wiley.com/terms-and-conditions) on Wiley Online Library for rules of use; OA articles are governed by the applicable Creative Commons License

Ćuk, M., Gladman, B. J., and Nesvorný, D. 2014. Hungaria Asteroid Family as the Source of Aubrite Meteorites. *Icarus* 239: 154–59.

Dauphas, N. 2017. The Isotopic Nature of the Earth's Accreting Material though Time. *Nature* 451: 521–24.

de Sousa, R. R., Morbidelli, A., Raymond, S. N., Izidoro, A., Gomes, R., and Neto, E. V. 2020. Dynamical Evidence for an Early Giant Planet Instability. *Icarus* 339: 113605.

DeMeo, F. E., Alexander, C. M. O'D., Walsh, K. J., Chapman, C. R., and Binzel, R. P. 2015. The Compositional Structure of the Asteroid Belt. In *Asteroids IV*, edited by P. Michel, F. E. DeMeo, and W. F. Bottke, 13–42. Tucson, AZ: The University of Arizona Press.

DeMeo, F. E., Binzel, R. P., Slivan, S. M., and Bus, S. J. 2009. An Extension of the Bus Asteroid Taxonomy into the Near-Infrared. *Icarus* 202: 160–180.

DeMeo, F. E., and Carry, B. 2014. Solar System Evolution from Compositional Mapping of the Asteroid Belt. *Nature* 505: 629–634.

Dodd, R. T. 1981. Chondritic Meteorites: A Changed and Changing View. *Nature* 290: 189–190.

Downes, H., Mittlefehldt, D. W., Kita, N. T., and Valley, J. W. 2008. Evidence from Polymict Ureilite Meteorites for a Disrupted and Re-accreted Single Ureilite Parent Asteroid Gardened by Several Distinct Impactors. *Geochimica et Cosmochimica Acta* 72: 4825–44.

El Goresy, A., Boyet, M., and Miyashara, M. 2011. Almahata Sitta EL-3 Chondrite Fragment: Contrasting Oldhamite Assemblages in Chondrules and Matrix and Significant Oldhamite REE Patterns. 74th Annual Meeting of the Meteoritical Society, abstract #5079.

El Goresy, A., Lin, Y., Feng, L., Boyet, M., Hao, J., Zhang, J., and Dubrovinsky, L. 2012. Almahata Sitta EH-3 Chondrites: Sinoite, Graphite, and Oldhamite (CaS) Assemblages C- and N-Isotopic Compositions and REE Patterns. 75th Annual Meeting of the Meteoritical Society, abstract #5108.

El Goresy, A., Lin, Y., Miyahara, M., Gannoun, A., Boyet, M., Ohtani, E., Gillet, P., et al. 2017. Origin of EL3 Chondrites: Evidence for Variable C/O Ratios During their Course of Formation—A State of the Art Scrutiny. *Meteoritics & Planetary Science* 52: 781–806.

Fagan, T. J., Scott, E. R. D., Keil, K., Cooney, T. F., and Sharma, S. K. 2000. Formation of Feldspathic and Metallic Melts by Shock in Enstatite Chondrite Reckling Peak A80259. *Meteoritics & Planetary Science* 35: 319–329.

Fioretti, A. M., Goodrich, C. A., Shaddad, M., Jenniskens, P., Zolensky, M., Kohl, I., Young, E., et al. 2017. A Report on 63 Newly Sampled Stones of the Almahata Sitta Fall (Asteroid 2008 TC_3) from the University of Khartoum Collection, Including a C2 Carbonaceous Chondrite. 48th Lunar and Planetary Science Conference, abstract #1846.

Fitoussi, C., and Bourdon, B. 2012. Silicon Isotope Evidence against an Enstatite Chondrite Earth. *Science* 335: 1477–80.

Fukuda, K., Tenner, T. J., Kimura, M., Tomioka, N., Siron, G., Ushikubo, T., Chaumard, N., Hertwig, A. T., and Kita, N. T. 2022. A Temporal Shift of Chondrule Generation from the Inner to Outer Solar System Inferred from Oxygen Isotopes and Al-Mg Chronology of Chondrules from Primitive CM and CO Chondrites. *Geochimica et Cosmochimica Acta* 322: 194–226.

Gayon-Markt, J., Delbo, M., Morbidelli, A., and Marchi, S. 2012. On the Origin of the Almahata Sitta Meteorite and 2008 TC_3 Asteroid. *Monthly Notices of the Royal Astronomical Society* 424: 508–518.

Goodrich, C. A., Bottke, W. F., Walsh, K. J., and Daly, R. T. 2021. Almahata Sitta Is no More Exotic than any Other Polymict Ureilite. 52nd Lunar and Planetary Science Conference, abstract #1331.

Goodrich, C. A., Collinet, M., Jercinovic, J., Prissel, T., Tang, H., Tafla, L., Young, E., Jenniskens, P., and Shaddad, M. H. 2022b. Almahata Sitta 3005: A New Sample of Ureilitic Crust and New Insights into Differentiation of the Ureilite Parent Asteroid. 53rd Lunar and Planetary Science Conference, abstract #1065.

Goodrich, C. A., Collinet, M., Treiman, A., Prissel, T. C., Patzek, M., Jercinovic, M. J., Ebert, S., et al. 2022a. The First Main-Group Ureilite with Primary Plagioclase: A Missing Link in the Differentiation of the Ureilite Parent Body. *Meteoritics & Planetary Science* 57: 1589–1616.

Goodrich, C. A., Fioretti, A. M., O'Brien, D. P., Zolensky, M., Jenniskens, P., and Shaddad, M. H. 2015. Comparing the Foreign Clast Populations of Almahata Sitta and Typical Polymict Ureilites, with Implications. 78th Annual Meeting of the Meteoritical Society, abstract #5018.

Goodrich, C. A., Fioretti, A. M., Zolensky, M., Shaddad, M., Ross, D. K., Kohl, I., Young, E., et al. 2018. The Almahata Sitta Polymict Ureilite from the University of Khartoum Collection: Classification, Distribution of Clast Types in the Strewn Field, New Meteorite Types, and Implications for the Structure of Asteroid 2008 TC_3. 49th Lunar and Planetary Science Conference, abstract #1321.

Goodrich, C. A., and Gross, J. 2015. A New Type of Ordinary Chondrite (?) Clast in a Polymict Ureilite. 46th Lunar and Planetary Science Conference, abstract #1214.

Goodrich, C. A., Hartmann, W. K., O'Brien, D. P., Weidenschilling, S., Wilson, L., Michel, P., and Jutzi, M. 2015. Origin and History of Ureilitic Material in the Solar System: The View from Asteroid 2008 TC_3 and the Almahata Sitta Meteorite. *Meteoritics & Planetary Science* 50: 782–809.

Goodrich, C. A., Hutcheon, I. D., Kita, N. T., Huss, G. R., Cohen, B. A., and Keil, K. 2010. ^{53}Mn-^{53}Cr and ^{26}Al-^{26}Mg Ages of a Feldspathic Lithology in Polymict Ureilites. *Earth and Planetary Science Letters* 295: 531–540.

Goodrich, C. A., Kita, N. T., Yin, Q.-Z., Sanborn, M. E., Williams, C. D., Nakashima, D., Lane, M. D., and Boyle, S. 2017. Petrogenesis and Provenance of Ungrouped Achondrite Northwest Africa 7325 from Petrology, Trace Elements, Oxygen, Chromium and Titanium Isotopes, and Mid-IR Spectroscopy. *Geochimica et Cosmochimica Acta* 203: 381–403.

Goodrich, C. A., Kring, D. A., and Greenwood, R. 2021. Xenoliths in Ordinary Chondrites and Ureilites: Implications for Early Solar System Dynamics. *Meteoritics & Planetary Science* 56: 1949–87.

Goodrich, C. A., Mikouchi, T., and Treiman, A. H. 2015. A Volcanic (Quenched) Angrite Clast in Polymict Ureilite DaG 319. 78th Annual Meeting of the Meteoritical Society, abstract #5048.

Goodrich, C. A., Ross, D. K., and Treiman, A. H. 2017. A New Type of Foreign Clast in a Polymict Ureilite: A CAI

19455100, 2024, 4, Downloaded from https://onlinelibrary.wiley.com/doi/10.1111/maps.14066 by University Of Wisconsin - Madison, Wiley Online Library on [18/06/2024]. See the Terms and Conditions (https://onlinelibrary.wiley.com/terms-and-conditions) on Wiley Online Library for rules of use; OA articles are governed by the applicable Creative Commons License

or Al-Rich Chondrule. 48th Lunar and Planetary Science Conference, abstract #1101.
Goodrich, C. A., Sanborn, M. E., Yin, Q.-Z., Kohl, I., Frank, D., Daly, R. T., Walsh, K. J., et al. 2021. Cr Isotopic Evidence for Mixing of NC and CC Reservoirs in Polymict Ureilites: Implications for Early Solar System Dynamics. *Planetary Science Journal* 2: 15.
Goodrich, C. A., Scott, E. R. D., and Fioretti, A. M. 2004. Ureilitic Breccias: Clues to the Petrologic Structure and Impact Disruption of the Ureilite Parent Body. *Chemie der Erde* 64: 283–327.
Goodrich, C. A., Treiman, A. H., and Boyle, S. 2017. Melt Formation and Evolution on the Ureilite Parent Body, as Shown by Feldspathic Clasts in Polymict Ureilites. 48th Lunar and Planetary Science Conference, abstract #1196.
Goodrich, C. A., Treiman, A. H., Kita, N. T., and Defouilloy, C. 2016. Increasing Diversity of Ordinary Chondrite and Rumuruti-Type Chondrite Clasts in Polymict Ureilites. 47th Lunar and Planetary Science Conference, abstract #1617.
Goodrich, C. A., Zolensky, M., Fioretti, A. M., Shaddad, M. H., Downes, H., Hiroi, T., Kohl, I., et al. 2019. The First Samples from Almahata Sitta Showing Contacts between Ureilitic and Chondritic Lithologies: Implications for the Structure and Composition of Asteroid 2008 TC_3. *Meteoritics & Planetary Science* 54: 2769–2813.
Goodrich, C. A., Zolensky, M., Kohl, I., Young, E. D., Yin, Q.-Z., Sanborn, M. E., and Shaddad, M. H. 2019. Carbonaceous Chondrite-Like Xenoliths in Polymict Ureilites: A Large Variety of Unique Outer Solar System Materials. 50th Lunar and Planetary Science Conference, abstract #1312.
Goss, K. R., Gray, M. L., Weisberg, M. K., and Ebel, D. S. 2023. Lewis Cliff 87223, an Anomalous Enstatite Chondrite and the Diversity of Enstatite Chondrites. *Meteoritics & Planetary Science* 58: 433–443.
Greenwood, R. C., Barrat, J.-A., Miller, M. F., Anand, M., Dauphas, N., Franchi, I. A., Sillard, P., and Starkey, N. A. 2018. Oxygen Isotopic Evidence for Accretion of Earth's Water before a High-Energy Moon-Forming Giant Impact. *Science Advances* 4: eaao5928.
Greenwood, R. C., Burbine, T. H., Miller, M. F., and Franchi, I. A. 2017. Melting and Differentiation of Early Formed Asteroids: The Perspective from High Precision Oxygen Isotope Studies. *Chemie der Erde* 77: 1–43.
Grossman, J. N., MacPherson, G. J., and Crozaz, G. 1993. LEW 87223: A Unique E Chondrite with Possible Links to H Chondrites. *Meteoritics* 28: 358.
Hamilton, V. E., Goodrich, C. A., Treiman, A. H., Connolly, H. C., Jr., Zolensky, M. E., and Shaddad, M. H. 2020. Meteoritic Evidence for a Ceres-Sized Water-Rich Carbonaceous Chondrite Parent Asteroid. *Nature Astronomy Letters* 5: 350–55.
Harries, D., and Bischoff, A. 2020. Petrological Evidence for the Existence and Disruption of a 500 km-Sized Differentiated Planetesimal of Enstatite-Chondritic Parentage. *Earth and Planetary Science Letters* 548: 116506.
Herrin, J. S., Zolensky, M. E., Ito, M., Le, L., Mittlefehldt, D. W., Jenniskens, P., Ross, A. J., and Shaddad, M. H. 2010. Thermal and Fragmentation History of Ureilitic Asteroids: Insights from the Almahata Sitta Fall. *Meteoritics & Planetary Science* 45: 1789–1803.
Hiroi, T., Jenniskens, P., Bishop, J. L., Shatir, T. S. M., Kudoda, A. M., and Shaddad, M. H. 2010. Bi-Directional Visible-NIR and Biconical FT-IR Reflectance Spectra of Almahata Sitta Meteorite Samples. *Meteoritics & Planetary Science* 45: 1836–45.
Horstmann, M. 2010. Mineralogy and Chemistry of Selected Components in Meteorites. Master thesis. Westfälische Wilhelms-Universität Münster. Münster, Germany.
Horstmann, M., and Bischoff, A. 2014. The Almahata Sitta Polymict Breccia and the Late Accretion of Asteroid 2008 TC_3. *Chemie der Erde* 74: 149–183.
Horstmann, M., Bischoff, A., Pack, A., Albrecht, N., Weyrauch, M., Hain, H., Roggon, L., and Schneider, K. 2012. Mineralogy and Oxygen Isotope Composition of New Samples from the Almahata Sitta Strewn Field. 75th Annual Meeting of the Meteoritical Society, abstract #5052.
Horstmann, M., Bischoff, A., Pack, A., and Laubenstein, M. 2010. Almahata Sitta Fragment MS-CH: Characterization of a New Chondrite Type. *Meteoritics & Planetary Science* 45: 1657–67.
Horstmann, M., Humayun, M., and Bischoff, A. 2011. Siderophile Element Patterns of Sulfide-Metal Assemblages from the Almahata Sitta Polymict Breccias. 74th Annual Meeting of the Meteoritical Society, abstract #5096.
Horstmann, M., Humayun, M., and Bischoff, A. 2014. Clues to the Origin of Metal in Almahata Sitta EL and EH Chondrites and Implications for Primitive E Chondrite Thermal Histories. *Geochimica et Cosmochimica Acta* 140: 720–744.
Huss, G. H., Rubin, A. E., and Grossman, J. N. 2006. In *Meteorites and the Early Solar System II*, edited by D. S. Lauretta, and H. Y. McSween, Jr., 567–586. Tucson, AZ: The University of Arizona Press.
Ikeda, Y., Kita, N. T., Morishita, Y., and Weisberg, M. K. 2003. Primitive Clasts in the Dar al Gani 319 Polymict Ureilite: Precursors of the Ureilites. *Antarctic Meteorite Research* 16: 105–127.
Ikeda, Y., Prinz, M., and Nehru, C. E. 2000. Lithic and Mineral Clasts in the Dar al Gani (DaG) 319 Polymict Ureilite. *Antarctic Meteorite Research* 13: 177–221.
Jaques, A. L., and Fitzgerald, M. J. 1982. The Nilpena Ureilite, an Unusual Polymict Breccia: Implications for Origin. *Geochimica et Cosmochimica Acta* 46: 893–900.
Jenniskens, P., Robertson, D., Goodrich, C. A., Shaddad, M. H., Kudoda, A., Fioretti, A. M., and Zolensky, M. E. 2022. Bolide Fragmentation: What Parts of Asteroid 2008 TC_3 Survived to the Ground? *Meteoritics & Planetary Sciences* 57: 1641–64.
Jenniskens, P., Shaddad, M. H., Numan, D., Elsir, S., Kudoda, A. M., Zolensky, M. E., Le, L., et al. 2009. The Impact and Recovery of Asteroid 2008 TC_3. *Nature* 458: 485–88.
Jenniskens, P., Vaubaillon, J., Binzel, R. P., Demeo, F. E., Desvorný, D., Bottke, W. F., Fitzsimmons, A., et al. 2010. Almahata Sitta (= Asteroid 2008 TC_3) and the Search for the Ureilite Parent Body. *Meteoritics & Planetary Science* 45: 1590–1617.
Keil, K. 1984. Enstatite Meteorites and their Parent Bodies. *Meteoritics* 24: 195–208.
Keil, K. 2007. Occurrence and Origin of Keilite ($Fe_{>0.5}$,$Mg_{<0.5}$) S in Enstatite Chondrite Impact-Melt Rocks and Impact-Melt Breccias. *Chemie der Erde* 67: 37–54.
Keil, K., and Bischoff, A. 2008. Northwest Africa 2526: A Partial Melt Residue of Enstatite Chondrite Parentage. *Meteoritics & Planetary Science* 43: 1233–40.
Keil, K., Ntaflos, T., Taylor, G. J., Brearley, A. J., Newsom, H. E., and Romig, A. D., Jr. 1989. The Shallowater

19455100, 2024, 4, Downloaded from https://onlinelibrary.wiley.com/doi/10.1111/maps.14066 by University Of Wisconsin - Madison, Wiley Online Library on [18/06/2024]. See the Terms and Conditions (https://onlinelibrary.wiley.com/terms-and-conditions) on Wiley Online Library for rules of use; OA articles are governed by the applicable Creative Commons License

Aubrite: Evidence for Origin by Planetesimal Impacts. *Geochimica et Cosmochimica Acta* 53: 3291–3307.

Kimura, M., Weisberg, M. K., Lin, Y., Suzuki, A., Ohtani, E., and Akazaki, R. 2005. Thermal History of the Enstatite Chondrites from Silica Polymorphs. *Meteoritics & Planetary Sciences* 40: 855–868.

Kimura, M., Weisberg, M. K., Takaki, A., Imae, N., and Yamaguchi, A. 2021. An Almahata Sitta EL3 Fragment: Implications for the Complex Thermal History of Enstatite Chondrites. *Progress in Earth and Planetary Science* 8: 55.

Kleine, T., Budde, G., Burkhardt, C., Kruijer, T. S., Worsham, E. A., Morbidelli, A., and Nimmo, F. 2020. The Non-carbonaceous-Carbonaceous Meteorite Dichotomy. *Space Science Reviews* 216: 55, 23 pp.

Kong, P., Mori, T., and Ebihara, M. 1997. Compositional Continuity of Enstatite Chondrites and Implications for Heterogeneous Accretion of the Enstatite Chondrite Parent Body. *Geochimica et Cosmochimica Acta* 61: 4895–4914.

Lin, Y., and Kimura, M. 1998. Petrographic and Mineralogical Study of New EH Melt Rocks and a New Enstatite Chondrite Grouplet. *Meteoritics & Planetary Science* 33: 501–511.

Lodders, K. 2000. An Oxygen Isotope Mixing Model for the Accretion and Composition of Rocky Planets. In From Dust to Terrestrial Planets: Proceedings of an ISSI Workshop, 15–19 February 1999, Bern, Switzerland. Springer Netherlands. pp. 341–54.

Lodders, K. 2003. Solar System Abundances and Condensation Temperatures of the Elements. *The Astrophysical Journal* 591: 1220–47.

McCoy, T. J., Keil, K., Bogard, D. D., Garrison, D. H., Casanova, I., Lindstrom, M. M., Brearley, A. J., Kehm, K., Nichols, R. H., Jr., and Hohenberg, C. M. 1995. Origin and History of Impact-Melt Rocks of Enstatite Chondrite Parentage. *Geochimica et Cosmochimica Acta* 59: 161–175.

Meier, M. M. M., Welten, K. C., Caffee, M. W., Friedrich, J. M., Jenniskens, P., Nishiizumi, K., Shaddad, M. H., and Wieler, R. 2012. A Noble Gas and Cosmogenic Radionuclide Analysis of Two Ordinary Chondrites from Almahata Sitta. *Meteoritics & Planetary Science* 47: 1075–86.

Michel, P., Benz, W., Tanga, P., and Richardson, D. C. 2001. Collisions and Gravitational Reaccumulation: Forming Asteroid Families and Satellites. *Science* 294: 1696–1700.

Michel, P., Jutzi, M., Richardson, D. C., Goodrich, C. A., Hartmann, W. K., and O'Brien, D. P. 2015. Selective Sampling during Catastrophic Disruption: Mapping the Location of Reaccumulated Fragments in the Original Parent Body. Proceedings of the 8th Catastrophic Disruption Workshop. Planetary and Space Science 107, 24–8.

Miller, M. F. 2002. Isotopic Fractionation and the Quantification of ^{17}O Anomalies in the Oxygen Three-Isotope System: An Appraisal and Geochemical Significance. *Geochimica et Cosmochimica Acta* 66: 1881–89.

Miyamoto, M., Fuji, N., and Takeda, H. 1981. Ordinary Chondrite Parent Body: An Internal Heating Model. 12th Lunar and Planetary Science Conference, pp. 1145–52.

Nehru, C. E., Prinz, M., Weisberg, M. K., and Delaney, J. S. 1984. Parsa: An Unequilibrated Enstatite Chondrite (UEC) with an Aubrite-like Impact Melt Clast. 15th Lunar and Planetary Science Conference, pp. 597–98.

Newton, J., Franchi, I. A., and Pillinger, C. T. 2000. The Oxygen-Isotopic Record in Enstatite Meteorites. *Meteoritics & Planetary Science* 35: 689–698.

Ott, U., Loehr, H. P., and Begemann, F. 1993. Solar Noble Gases in Polymict Ureilites and an Update on Ureilite Noble Gas Data. *Meteoritics* 28: 415–16.

Patzek, M., Bischoff, A., Visser, R., and John, T. 2018. Mineralogy of Volatile-Rich Clasts in Brecciated Meteorites. *Meteoritics & Planetary Science* 53: 2519–40.

Patzer, A., Hill, D. H., and Boynton, W. V. 2001. Itqiy: A Metal-Rich Enstatite Meteorite with Achondritic Texture. *Meteoritics & Planetary Science* 36: 1495–1505.

Pellas, P., and Fiéni, C. 1988. Thermal Histories of Ordinary Chondrite Parent Asteroids. 18th Lunar and Planetary Science Conference, 915.

Popova, O., Borovička, J., Hartmann, W. K., Spurný, P., Gnos, E., Nemtchinov, I., and Trigo-Rodríguez, J. M. 2011. Very Low Strengths of Interplanetary Meteoroids and Small Asteroids. *Meteoritics & Planetary Science* 46: 1525–50.

Prinz, M., Weisberg, M. K., Nehru, C. E., and Delaney, J. S. 1985. Layered Chondrules: Evidence for Multistage Histories during Chondrule Formation. *Meteoritics* 20: 732–33.

Prinz, M., Weisberg, M. K., Nehru, C. E., and Delaney, J. S. 1986. North Haig and Nilpena: Paired Polymict Ureilites with Angra dos Reis-Related and Other Clasts. 17th Lunar and Planetary Science, pp. 681–2.

Prinz, M., Weisberg, M. K., Nehru, C. E., and Delaney, J. S. 1987. Black Inclusions of Carbonaceous Chondrite Matrix Material in Polymict Ureilites. *Meteoritics* 22: 482–83.

Rai, N., Downes, H., and Smith, C. 2020. Ureilite Meteorites Provide a New Model of Early Planetesimal Formation and Destruction. *Geochemical Perspective Letters* 14: 20–25.

Riebe, M. E. I., Welten, K. C., Meier, M. M. M., Wieler, R., Barth, M. I. F., Ward, D., Laubenstein, M., et al. 2017. Cosmic Ray Exposure Ages of Six Chondritic Almahata Sitta Fragments. *Meteoritics & Planetary Science* 52: 2353–74.

Rindlisbacher, M. A., Weisberg, M. K., Ebel, D. S., and Alpert, S. P. 2021. Metal-Rich Nodules in Anomalous EL3 Chondrite Northwest Africa (NWA) 8785. *Meteoritics & Planetary Science* 56: 960–970.

Ross, A. J., Downes, H., Smith, C. L., and Jones, A. P. 2010. DaG 1047: A Polymict Ureilite Containing Exotic Clasts Including a Chondrite. 41st Lunar and Planetary Science, abstract #2361.

Rubin, A. 1997. The Galim LL/EH Polymict Breccia: Evidence for Impact Induced Exchange between Reduced and Oxidized Meteoritic Material. *Meteoritics & Planetary Science* 32: 489–492.

Rubin, A. E. 2015. Impact Features of Enstatite-Rich Meteorites. *Chemie der Erde* 75: 1–28.

Rubin, A. E., and Scott, E. R. D. 1997a. Abee and Related EH Chondrite Impact-Melt Breccias. *Geochimica et Cosmochimica Acta* 61: 425–435.

Rubin, A. E., and Scott, E. R. D. 1997b. Shock Metamorphism of Enstatite Chondrites. *Geochimica et Cosmochimica Acta* 61: 847–858.

Scott, E. R. D., Krot, A. N., and Sanders, I. S. 2018. Isotopic Dichotomy among Meteorites and its Bearing on the Protoplanetary Disk. *The Astrophysical Journal* 854: 164 (12 pp).

Shaddad, M. H., Jenniskens, P., Numan, D., Kudoda, A. M., Elsir, S., Riyad, I. F., Ali, A. E., et al. 2010. The Recovery of Asteroid 2008 TC_3. *Meteoritics & Planetary Science* 45: 1557–89.

19455100, 2024, 4, Downloaded from https://onlinelibrary.wiley.com/doi/10.1111/maps.14066 by University Of Wisconsin - Madison, Wiley Online Library on [18/06/2024]. See the Terms and Conditions (https://onlinelibrary.wiley.com/terms-and-conditions) on Wiley Online Library for rules of use; OA articles are governed by the applicable Creative Commons License

Shimizu, M., Yoshida, H., and Mandarino, J. A. 2002. The New Mineral Species Keilite, (Fe,Mg)S, the Iron-Dominant Analogue of Niningerite. *The Canadian Mineralogist* 40: 1687–92.

Sikdar, J., and Rai, V. K. 2020. Si-Mg Isotopes in Enstatite Chondrites and Accretion of Reduced Planetary Bodies. *Nature, Scientific Reports* 10: 1273.

Storz, J., Ludwig, T., Bischoff, A., Schwarz, W., and Trieloff, M. 2021. Graphite in Ureilites, Enstatite Chondrites, and Unique Clasts in Ordinary Chondrites—Insights from the Carbon-Isotope Composition. *Geochimica et Cosmochimica Acta* 307: 86–104.

Tholen, D. J., and Barucci, M. 1989. Asteroid Taxonomy. In *Asteroids II*, edited by R. Binzel, T. Gehrels, and M. Matthews, 298–315. Tucson, AZ: University of Arizona Press.

Trieloff, M., Hopp, J., and Gail, H.-P. 2022. Evolution of the Parent Body of Enstatite (EL) Chondrites. *Icarus* 373: 114762.

Turrin, B. D., Lindsay, F., Delaney, J. S., Park, J., Herzog, G. F., Swisher, C., Jr., and Goodrich, C. A. 2023. $^{40}Ar/^{39}Ar$ Ages of L4, H5, EL6, and Feldspathic Ureilitic Clasts from the Almahata Sitta Polymict Ureilite (Asteroid 2008 TC_3). *Meteoritics & Planetary Science* 58: 304–327.

Udry, A., Wilbur, Z. E., Rahib, R. R., McCubbin, F. M., Vander, K. K., E., McCoy, T. J., Ziegler, K., et al. 2019. Reclassification of Four Aubrites as Enstatite Chondrite Impact Melts: Potential Geochemical Analogs for Mercury. *Meteoritics & Planetary Science* 54: 785–810.

Van Niekerk, D., and Keil, K. 2011. Metal/Sulfide-Silicate Intergrowth Textures in EL3 Meteorites: Origin by Impact Melting on the EL Parent Body. *Meteoritics & Planetary Science* 46: 1484–97.

Walker, R. J., Bermingham, K., Liu, J., Puchtel, I. S., Touboul, M., and Worsham, E. A. 2015. In Search of Late-Stage Planetary Building Blocks. *Chemical Geology* 411: 125–142.

Walsh, K. J., Morbidelli, A., Raymond, S. N., O'Brien, D. P., and Mandell, A. M. 2012. Populating the Asteroid Belt from Two Parent Source Regions Due to the Migration of Giant Planets—"the Grand Tack". *Meteoritics & Planetary Science* 47: 1941–47.

Warren, P. H. 2011. Stable Isotopes and the Noncarbonaceous Derivation of Ureilites, in Common with Nearly all Differentiated Planetary Materials. *Geochimica et Cosmochimica Acta* 75: 6912–26.

Wasson, J. T., Choi, B.-G., Jerde, E., and Ulff-Møller, F. 1998. Chemical Classification of Iron Meteorites: XII. New Members of the Magmatic Groups. *Geochimica et Cosmochimica Acta* 62: 715–724.

Wasson, J. T., Huber, H., and Malvin, D. J. 2007. Formation of IIAB Iron Meteorites. *Geochimica et Cosmochimica Acta* 71: 760–781.

Wasson, J. T., Ouyang, X., Wang, J., and Jerde, E. 1989. Chemical Classification of Iron Meteorites: XI. Multi-Element Studies of 38 New Irons and the High Abundance of Ungrouped Irons from Antarctica. *Geochimica et Cosmochimica Acta* 53: 735–744.

Weisberg, M. K., and Kimura, M. 2012. The Unequilibrated Enstatite Chondrites. *Chemie der Erde* 72: 101–115.

Weisberg, M. K., Kita, N. T., Fukuda, K., Siron, G., and Ebel, D. S. 2021. Micro-Distribution of Oxygen Isotopes in Unequilibrated Enstatite Chondrites. *Geochimica et Cosmochimica Acta* 300: 279–295.

Welten, K. C., Meier, M. M. M., Caffee, M. W., Nishiizumi, K., Wieler, R., Jenniskens, P., and Shaddad, M. H. 2010. Cosmogenic Nuclides in Almahata Sitta Ureilites: Cosmic-Ray Exposure Age, Pre-Atmospheric Mass, and Bulk Density of Asteroid 2008 TC_3. *Meteoritics & Planetary Science* 45: 1728–42.

Weyrauch, M., Horstmann, M., and Bischoff, A. 2018. Chemical Variations of Sulphides and Metal in Enstatite Chondrites—Introduction of a New Classification Scheme. *Meteoritics & Planetary Science* 53: 394–415.

Wheelock, M. M., Keil, K., Floss, C., Taylor, G. J., and Crozaz, G. 1994. REE Geochemistry of Oldhamite-Dominated Clasts from the Norton County Aubrite: Igneous Origin of Oldhamite. *Geochimica et Cosmochimica Acta* 58: 449–458.

Wieler, R., Baur, H., and Signer, P. 1986. Noble Gases from Solar Energetic Particles Revealed by Closed System Stepwise Etching of Lunar Soil Minerals. *Geochimica et Cosmochimica Acta* 50: 1997–2017.

Yamakawa, A., Yamashita, K., Makashima, A., and Nakamura, E. 2010. Chromium Isotope Systematics of Achondrites: Chronology and Isotopic Heterogeneity of the Inner Solar System Bodies. *The Astrophysical Journal* 720: 150–54.

Zhang, Y., Benoit, P. H., and Sears, D. W. G. 1995. The Classification and Complex Thermal History of the Enstatite Chondrites. *Journal of Geophysical Research* 100: 9417.

Zhu, K., Moynier, F., Schiller, M., and Bizzarro, M. 2020. Dating and Tracing the Origin of Enstatite Chondrite Chondrules with Cr Isotopes. *The Astrophysical Journal Letters* 894: L26.

Zolensky, M., Herrin, J., Mikouchi, T., Ohsumi, K., Friedrich, J., Steele, A., Rumble, A., et al. 2010. Mineralogy and Petrography of the Almahata Sitta Ureilite. *Meteoritics & Planetary Science* 45: 1618–37.

SUPPORTING INFORMATION

Additional supporting information may be found in the online version of this article.

Figure S1. SIMS analysis locations and pit images of AhS 60.

Table S1. Oxygen isotope analyses of AhS 60 using SIMS IMS 1280. Raw data are Faraday cup background and OH tailing corrected.

19455100, 2024, 4, Downloaded from https://onlinelibrary.wiley.com/doi/10.1111/maps.14066 by University Of Wisconsin - Madison, Wiley Online Library on [18/06/2024]. See the Terms and Conditions (https://onlinelibrary.wiley.com/terms-and-conditions) on Wiley Online Library for rules of use; OA articles are governed by the applicable Creative Commons License